PARAMETERIZATION OF RADIATIVE TRANSFER AT ECMWF

by

J.-F. GELEYN

EUROPEAN CENTRE FOR MEDIUM RANGE WEATHER FORECASTS

LIST OF CONTENTS PAGE

LIST OF CONTENTS (contd.) PAGE

-.-.-.-.-

1. Applications of Radiative Computations to Numerical Forecasting

1.1 The basic problem

Unlike the other lecture on radiation given at this seminar, ours is not devoted to general problems but to the solutions we have chosen at ECMWF to answer a given question in a precise context.

Our goal is to develop a 10-day forecasting model and therefore the question mentioned above is: how can a radiative model be of some help for our more general task? But of course it would be a rather short term point of view to work with the only principle that all insignificant features for the dynamical forecast should be kept out of our radiative computation. A better attitude, and one which prepares for the future, is to say: all characteristics, which do not go in any way against our main purpose and which can help us to get a better understanding of radiative problems, ought to be implemented in our scheme. By "in any way" we understand that we should neither get wrong feedbacks with the dynamic, nor increase significantly the computer time or memory space consumption, nor bring impossible requirements for our input. As we are only now starting global integrations with our scheme included, it is obvious that so far the way we referred to our principles was subjective and that we might now have to change some features of our program, but we hope that at least its general frame is suitable and will be kept.

The constraints imposed on our task by the ECMWF's problem are of three kinds which can be described by the vague terms of technical, practical and physical.

- The technical limitations are related to the type of computer we are going to use and, in our case of a vector machine, to the way in which the radiation subroutine will be called. On the basis of time and space scales, whose choice will be explained later on, and with the condition of four minutes for radiation computations per day of integration, we get the requirements of 100 radiation runs for a vertical column (probably 15 levels) per second on the CRAY. This would lead to about 10 runs per second on our development computer (CDC 6600) if there were no vectorization possibilities in our code. Of course these requirements are probably over-estimated, but it is better to come to a situation where you can do more than expected than the reverse. We aimed towards this kind of goal with a special interest in making the code as vectorizable as possible. Vectorization means (in oversimplification) long but simple inner loops without conditional statements. One can either take separately each point where radiation fluxes are computed and vectorize the vertical loops, or take all points along a latitude circle at the same time and do all operations in horizontal loops, which are, of course, all vectorizable. But in this case we would

need an enormous amount of memory space to store the intermediate results if the computation is not presented in a way which minimises the informative variables. To leave both possibilities open we designed our scheme with a very general formulation for which there is no difference between all the layers along the vertical and with periodic regroupment of the information in a small number of coefficients. In any case some mixing between both ways of vectorization will be needed, but which one should take the leading role has yet to be decided. This decision is more difficult than a simple test of feasibility and efficiency since it interferes with the choice of the time and space interpolation procedure: if we vectorize horizontally we must group radiative computations along latitude circles at the same time step in order to be most efficient; in the other case we can pick out some points at each time step where we like. The model which will be presented here can do now (before optimisation of the code) 8 runs per second on the CDC 6600 with 15 levels. This feature is very dependent on the number and the vertical distribution of cloudy layers, therefore it should be taken only as an estimate and the final time constraint will depend on the cloud modelisation and on the way the global model reacts to it.

- The practical constraints can be summed up by: putting the accent on what should be important for a 10-day forecast. But here again the question is not as simple as it first looks: firstly, we do not know to what extent our forecast will be successful and whether the useful information will be limited to the conventional height charts and so on, or if some direct radiative variables, such as the flux at the ground, or straightforward consequences, for example the extremum soil temperatures, will be added; secondly, the first guess for our analysis system will be a forecast and it may be that an important systematic error, let us say in the stratosphere (region where measurements are uncertain and with little influence on the synoptic situation) would have no impact on the quality of a given forecast, but by cumulation would affect all forecasts after a certain time. However, the results of our first experiments confirm what other people have already pointed out: the impact of radiation on a medium range forecast is localised mainly in the boundaries. It is easy to understand that the flux at the soil will have an important effect on the forecast because it fixes the surface temperature (on continents only) and therefore the rates of soil-atmosphere exchanges of heat, moisture and momentum. For the fluxes at the top of the atmosphere (the radiative balance) the argument is less obvious: the effects of a change there tend to concentrate in the stratosphere where feedback mechanism through other physical processes are missing. According to this situation, we chose to design a radiation scheme in which the accent is put more on the fluxes than on their divergences and therefore more on scattering than on absorption. This needs a more general development of the basic equation of radiative transfer than the ones which are generally used in radiative

computations, but this disadvantage can be compensated by the use of simplifications which only seriously affect the evaluation of gaseous absorption. The more important scattering agents in the atmosphere are the clouds; therefore our model is able to treat clouds with any partial coverage in all model layers and we hope that the cloud-diagnostic method in experimentation will produce a suitable input for our computations.

- The physical need we had in implementing our radiation scheme was to allow a maximum of consistency with other parts of the ECMWF physical package. Of course, this is not a one way process and compromises are necessary on all questions, but our main guideline was that a model which can deal with a maximum of information without any theoretical frame relative to the extra ones (internal consistency in a certain sense) will be easily transformed to deal only with the basic ones. This is even more valid if we apply the ideas of generality and simplicity expressed about the technical limitations and particularly on the treatment of the input information.

From the three answers given above to the constraints of 10-day forecasting we can notice that all three have something to do with "generalisation", though in different meanings of the word. In fact this was our main guideline and the result is a code in which all the important non-physical computations are done in only two couples (1 for long waves - 1 for short waves) of subroutines: the first ones are for local transmissivities, reflectivities and emissivities and the second ones for vertical combinations of these properties. The physical computations are either concentrated at the beginning for Rayleigh effect, clouds and aerosols, or at the end for gaseous absorptions and do not bring any complications of the code. This simplicity makes the program an easy tool for theoretical radiation studies in the frame of a global model since its features can be changed without compatibility problems. Of course, as the code is rather compact, the theoretical way to explain it is quite long and sometimes cumbersome.

All that has been mentioned in this kind of introduction is relative to the one peculiar answer among many other possibilities we gave to our basic question, and the process of creating the scheme was not as simple as it has been sketched here. Many people interacted through discussion, criticism and suggestions in a complicated development that we will now describe and justify later. We will try first to explain the reasons for this complexity.

1.2 Special features of radiation parameterization as compared with other parameterizations

Among other parameterisations (boundary layer, convection, condensation and precipitation, soil processes ...) radiation holds a very special situation: it is not computed in all cases, its impact is difficult to evaluate although

it has no stability problems, and it needs a boundary condition at infinity plus considerable climatological data. All these features, which make a complex problem of evaluating the quality of a radiation scheme, will be detailed now.

First of all, the average response time of atmospheric temperature to radiative divergences is far longer than those of humidity to convection and rainfall and of wind to turbulent mixing. The ratios are difficult to evaluate but probably of the same order of magnitude as the ones between the renewal times of internal energy by radiation and latent energy by rainfall-evaporation (1/12) and of the former, and kinetic energy by generation-dissipation (1/17). This means that there is no reason to compute radiative flux fields at every time step of the model, as is the case for other physical processes. This is a fortunate situation in view of the cost of radiative computations which is an order of magnitude higher than that of the remaining physical package. Of course this average situation is not true at the soil level and in its neighbourhood if we want to simulate the diurnal cycle on continents. We then have to find a process to simulate the changes of the fluxes with temperature, solar zenith angle and, if possible, cloudiness, without redoing the whole computation. This is the time interpolation problem. The question of whether it is worth doing or not is an important one. From the radiative point of view there is no doubt that the introduction of a diurnal cycle in the model will bring an improvement in our tools for the study of the feed back processes between radiation and other phenomena. For the dynamical results, some experiments with other models show that its influence should be little, but as already mentioned, the study of parameters near the ground may be interesting for the users if the global forecast has already shown a good quality. However, this feature is easy to switch on or off and thus we first want to try it in consistency with a boundary layer formulation in which fluxes are dependent on stability.

The time spacement problem is closely related with a similar one in space: if our simulation of the changes occuring between two radiation computations with respect to prognostic variables, such as temperature and humidity, is of poor quality or non-existent, it is likely, with a small-mesh grid, that a computation in each point does not bring any improvement against one done only in some selected points or with locally averaged values. Due to advection, the situation in one given point at the end of a period without radiation computation may be closer to the beginning situation in a neighbour point as in itself and so a wrong way of interaction with ampliciation of small waves may be induced. So we have to choose a grid size for radiation computations related to their time scale and this probably implies, in the case of ECMWF dynamical mesh, that we need a space interpolation procedure which of course is interdependent with the time interpolation one. This may be easy to implement in the East-West direction (we would have had to do it anyway in this direction to

reduce the number of radiative points while going polewards), but some difficulties will probably arise in the North-South direction due to the simultaneous presence of only three latitude rows in the memory. All this has still to be decided as experiments with the whole model are necessary to do it.

One other special feature of the radiative parameterisation is that its testing is rather difficult in practice. The effects of radiation are either weak (in the atmosphere) but not negligible because cumulative, or strong (at the soil on continents) but periodical with partial compensation. Therefore tests are very expensive, because for the first feature long and global integrations are necessary, and for the second one a sophisticated model for other parameterisations and a good tuning of the soil parameters are needed to simulate some locally observed situation with a one dimensional model. In both cases it is impossible to draw conclusions from the experiments without a good understanding of the main feedback effects which took place in them.

This situation is very well illustrated by the example shown in Figures 1 to 4 taken from Walker (1977). Four 72 hour forecasts for the GATE area are characterised by the third day total rainfall and they differ by the type of clouds (interactive) which are included in the radiation input. On the continent the most important changes occur when layer clouds are suppressed: the evaporation due to solar heating of the soil is increased. On the ocean the removal by convective clouds is far more important than the one of layer clouds: the long wave cooling associated with the top of penetrating convection columns enhance condensation. Of course there are also interactions between these two kinds of behaviour but they remain very easy to notice on the four comparative figures.

But this unfortunate situation also has its advantages: the changes in temperature being either cumulative or damped there is no stability problem for the numerical integration of the radiative terms and they can be computed explicitly and without limitation in opposition to all other physical terms: vertical diffusion must be done implicitly, horizontal diffusion, though explicit, must be kept within some limits, rainfall and convection, if computed explicitly instead of diagnostically adjusted, must not be allowed to go mathematically over their physical sources and sinks. This difference can be explained very easily: the atmosphere in general is far from its radiative equilibrium situation but quite near to vertical neutrality and to absence of clouds.

However, the main special feature of radiation is that it is the only way the earth-atmosphere system can exchange energy with the outside. This alone explains the necessity of introducing radiation in a meteorological forecast but brings a technical difficulty: the need of a flux at pressure zero which is an undefined level at infinity. In fact the distribution of the variables along the vertical creates a difficulty only for the temperature: what shall we use as T_∞ for the input of the radiative code ? There are a lot of possibilities (extrapolation,

Figure 1

INTERACTIVE RADIATION WITH CONVECTIVE CLOUDS

EXPNO: 5000
FORECAST: 72HRS. TO 12Z 7/ 9/74

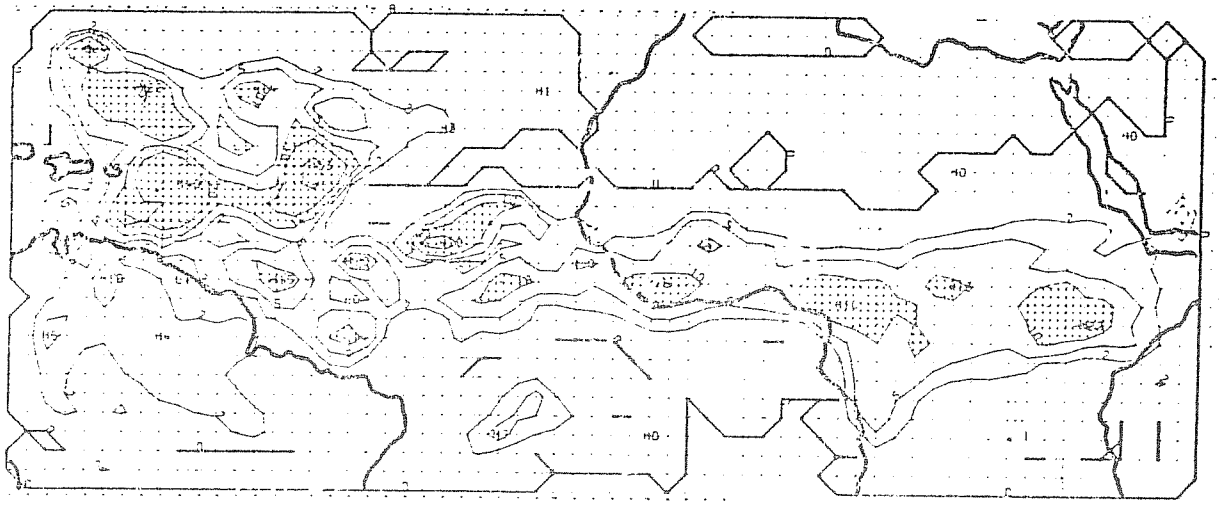

TOTAL RAIN (ZEROED EVERY 24HRS.)
LEVEL: SURFACE

INTERACTIVE RADIATION WITH ALL CLOUDS

EXPNO: 4000
FORECAST: 72HRS. TO 12Z 7/ 9/74

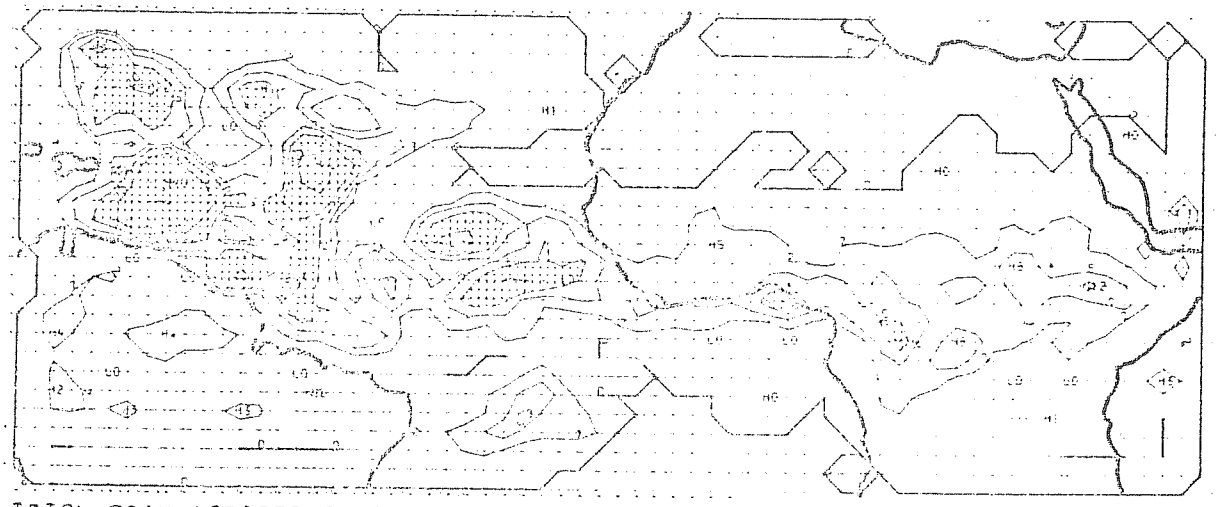

TOTAL RAIN (ZEROED EVERY 24HRS.)
LEVEL: SURFACE

Walker, 1977

Figure 2

INTERACTIVE RADIATION WITH LAYER CLOUDS

EXPNO: 6000
FORECAST: 72HRS. TO 12Z 7/ 9/74

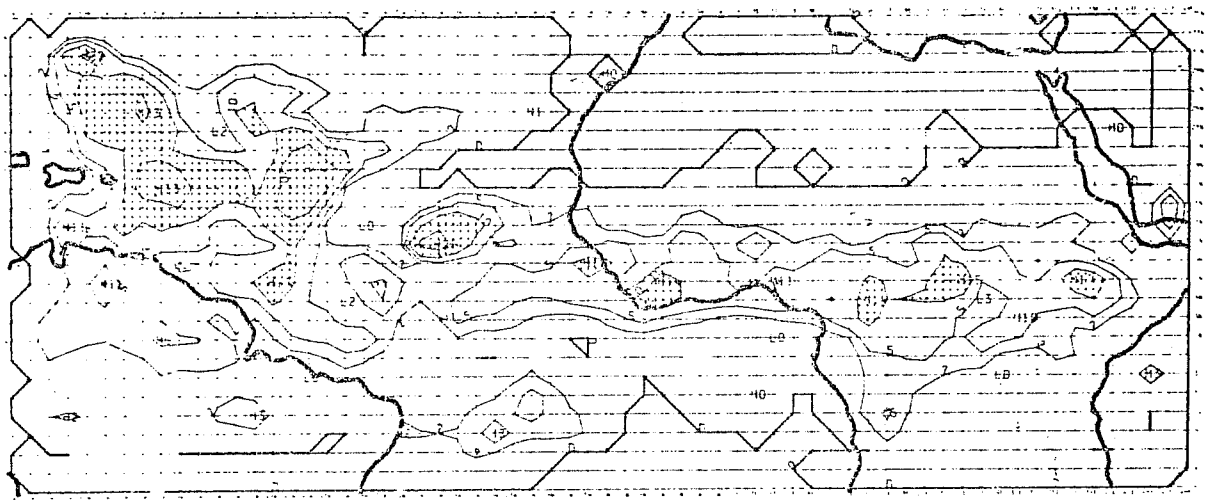

TOTAL RAIN (ZEROED EVERY 24HRS.)
LEVEL: SURFACE

INTERACTIVE RADIATION WITH ALL CLOUDS

EXPNO: 4000
FORECAST: 72HRS. TO 12Z 7/ 9/74

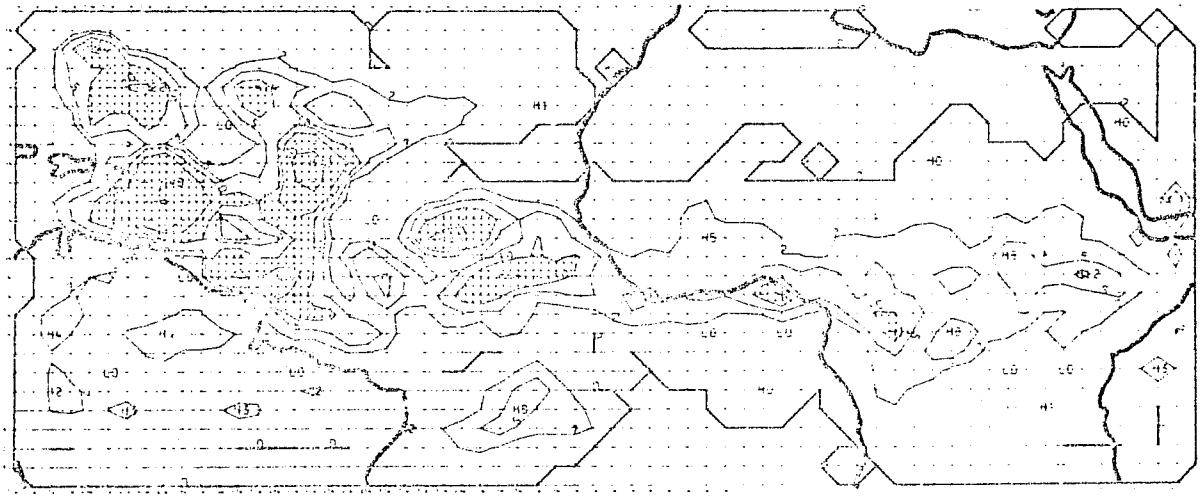

TOTAL RAIN (ZEROED EVERY 24HRS.)
LEVEL: SURFACE

Walker, 1977

Figure 3

INTERACTIVE RADIATION WITH CLEAR SKIES

EXPNO: 3000
FORECAST: 72HRS. TO 12Z 7/ 9/74

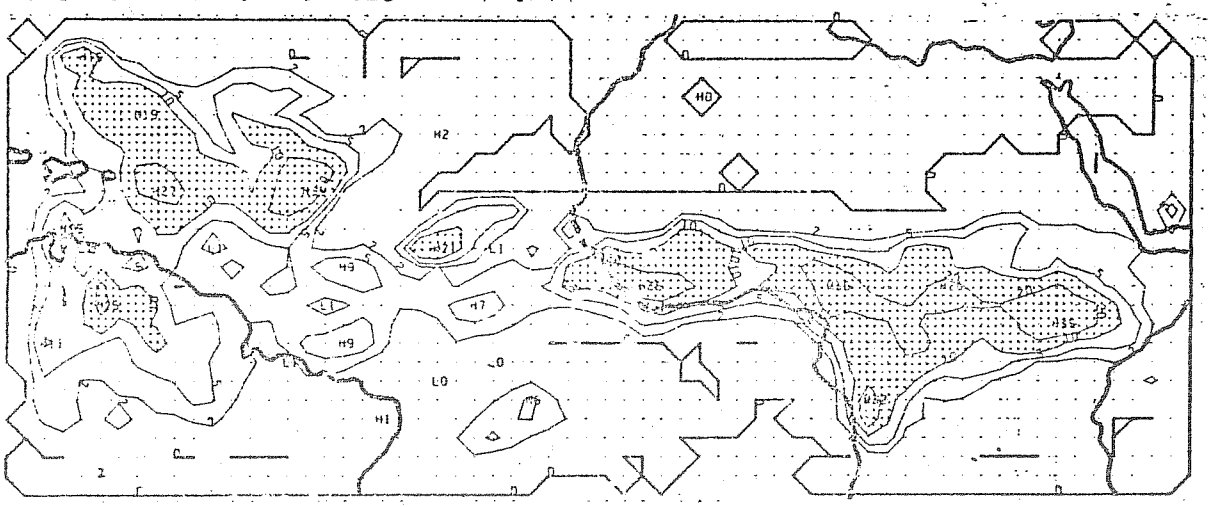

TOTAL RAIN (ZEROED EVERY 24HRS.)
LEVEL: SURFACE

INTERACTIVE RADIATION WITH CONVECTIVE CLOUDS

EXPNO: 5000
FORECAST: 72HRS. TO 12Z 7/ 9/74

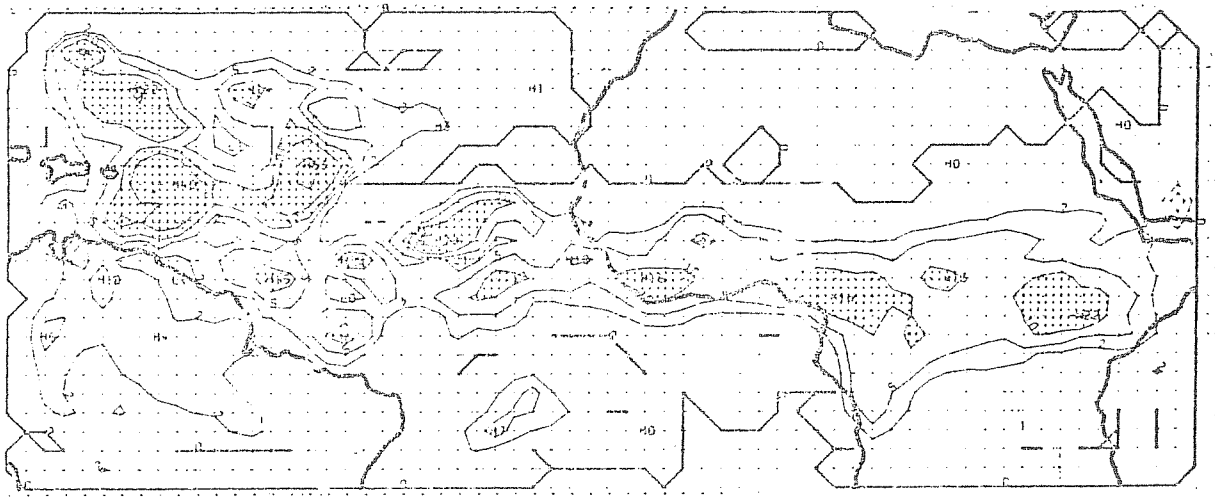

TOTAL RAIN (ZEROED EVERY 24HRS.)
LEVEL: SURFACE

Walker, 1977

Figure 4

INTERACTIVE RADIATION WITH CLEAR SKIES

EXPNO: 3000
FORECAST: 72HRS. TO 12Z 7/ 9/74

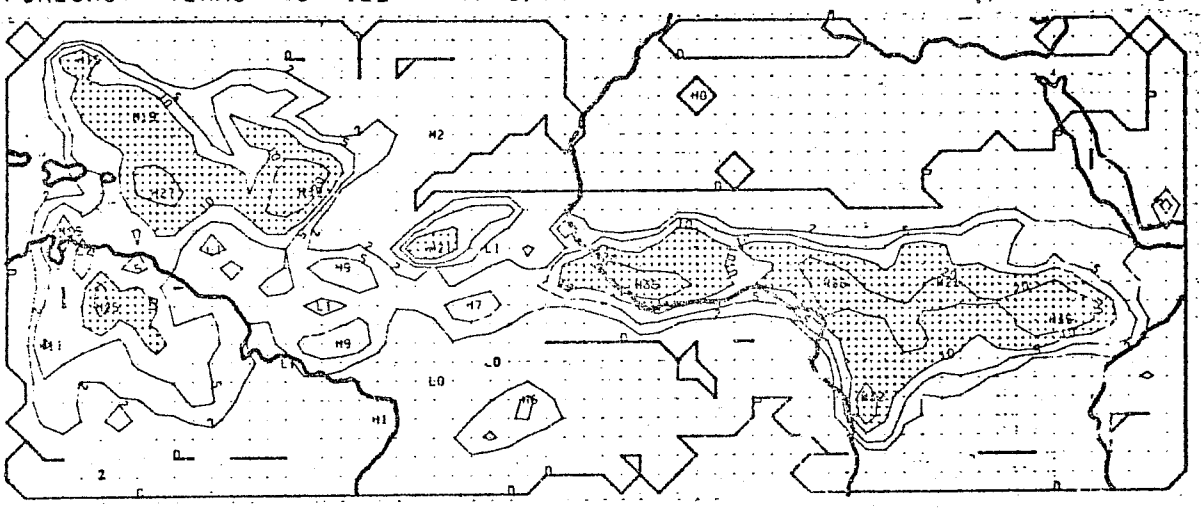

TOTAL RAIN (ZEROED EVERY 24HRS.)
LEVEL: SURFACE

INTERACTIVE RADIATION WITH LAYER CLOUDS

EXPNO: 6000
FORECAST: 72HRS. TO 12Z 7/ 9/74

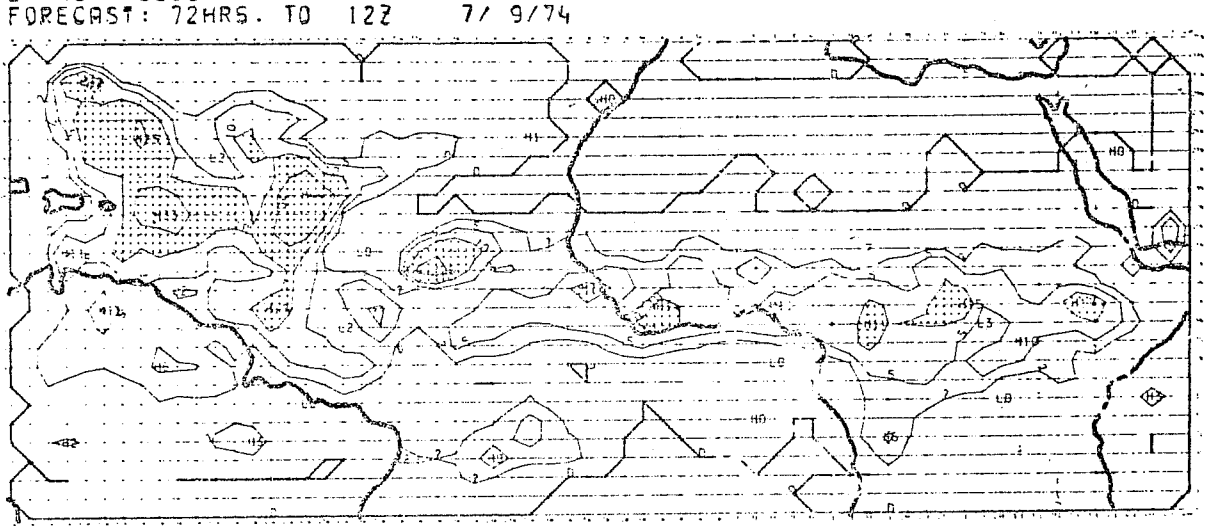

TOTAL RAIN (ZEROED EVERY 24HRS.)
LEVEL: SURFACE

Walker, 1977

"climatological" values, diagnostic or prognostic from the fluxes, replacement of the temperature condition by a flux condition ...) and, as already mentioned, the global model is quite sensitive to this choice since differences tend first to concentrate in the upper atmosphere. This because the downward long wave flux at infinity remains zero whatever T_∞ is and this parameter therefore mainly works on the outcoming fluxes of the last layer. So with a fixed boundary value of temperature a discontinuity arises and with an extrapolated value there is a kind of instability which occurs if the first layer induces changes quickly enough in the next one below. Surprisingly, there is no report of a comprehensive study of this problem by other modelling groups using radiation schemes for global integrations (however, this would perhaps be useless because the results must be very sensitive to the modelisation of both radiation and other physical processes) and we will have to find something suitable for our model.

The "mathematical" question of temperature at infinity is particularly annoying as we have no "physical" guideline to solve it but there are a lot of other input-output problems which, without this special difficulty, are also important for the radiative computations. There is a lack of basic information, both on climatological parameters and on the signification of the communication between the global model and the radiative scheme. The first feature is symptomatic of all our difficulties: we must include the effects of ozone, carbon dioxide and aerosols because they are important, but, especially for aerosols, the knowledge of their global distribution in space and time and of their optical properties is far behind the level required to match the supposed accuracy of the part of the code relative to data coming from the global model. Fortunately, this problem should not be crucial for a 10-day forecast and our policy for aerosols was to include, in an oversimplified manner, all their features which can have some effect and to leave a few parameters open to allow tuning with empiric goals (a change in the aerosol properties can correct a wrong flux balance at the top of the atmosphere). Although easier to study, the second feature may bring us more difficulties than the first one. It is essentially related to the clouds: for simplicity reasons we must assume that cloud layers have the vertical extension of the associated model layers; thus the cloudiness parameters must be more or less an expression of the amount of cloud inside the layer and may have little to do with the "measured" cloudiness, the real test of validity being the horizontally averaged fluxes below and above the cloudy layers for which of course very few measurements are available. Also the way in which these fluxes will act on the cloud processes by their divergences computed through the same model layers may lead to a wrong feed back.

After this review of the special features of radiation parameterisation we will express in the last three paragraphs of this chapter the general guidelines which we have given ourselves so far for the practical design and use of the scheme.

1.3 Time and space scales of integration

As seen before, the time scale is mainly related to the implementation of a diurnal cycle in the model. The question is then how many computations per day are necessary to get the main characteristics of the flux variations and allow a satisfactory time interpolation. To evaluate the needs let us take an oversimplified scheme: the fluxes are the sum of a full time part which vary linearly with time and a day time part defined by a maximum intensity and a proportionality to the solar zenity angle. This latter having three degrees of freedom we come to a total of six. This would mean six runs per day, but if we consider that four of the parameters cannot be determined at night, we come to eight computations per cycle or to hybrid systems in which more computations are done at day time than at night or the long wave and short wave parts get different frequencies. Of course, this is only a very schematic evaluation and the lapse time of three to four hours should only be considered as an order of magnitude. An interesting coincidence in the case of the ECMWF model is that then the ratio of the radiation time step to the dynamical one (about 15 minutes) would be of the same order of magnitude as the ratios of time renewals given earlier. Of course in the future if we decide to go further on and to allow the incorporation of cloudiness in the time interpolation process, the increase in the number of degrees of freedom would probably make a reduction of the time lapse necessary and therefore this improvement will only be possible if the vectorization of the code has brought about more time reduction than expected, which is very unlikely. One could also think of a simplification of the code, but then the cloudiness data must lose a good deal of their informative value and we think that it would not be worth doing.

With a mean wind speed of 17 m/s a 4 hour lapse time gives us a grid mesh of 350 Km and this means about 25000 column computations for a one-day integration, which leads us to the feature given at the beginning of 100 runs per second, corresponding to a necessary vectorization improvement of 1.2. The results for a 3 hour lapse time are 260 Km, 59000 computations, 240 runs per second and a factor 3, not out of range. In practice the grid size will be dependent on the one of the global model (about 125 Km) and the results above show that it will probably be either its double or the latter's product by $\sqrt{2}$ at the equator, with a decrease in the number of computational points along a latitude circle when going polewards.

All this will need confirmation by trials in the frame of the whole model and we may have to change our point of view if the interaction processes require it.

1.4 Significance of radiation computations

First we should point out that the kind of significance we are looking for is not exactly the same one as expressed in the other lecture on radiation at this seminar. Some features may be important for the accuracy of radiative computation but have no influence at all on a forecast because of strong damping by other phenomena and the reverse, though unlikely could be true in some extreme situations.

It is certainly this notion of extreme situations which we must always keep in mind when discussing significance: the impact of radiation on long waves and zonal flow at a large time scale and on micro-meteorology at a short time scale has been recognized for a long time, but there seems to be a gap between these two effects; however this gap does not mean the absence of processes and the sensitivity of radiation to clouds which are strongly correlated with synoptic waves suggests that some interaction should exist at this level and it may become important in some extreme situations. This is confirmed by another example taken from Walker (1977) and shown in Figure 5. Two 5 day integrations of nearly the same model are illustrated by surface pressure charts, the only difference being that the cloud input for radiation is either interactive or climatological. One can see that the main change is in the intensity and in the position of the low pressure centres. In the interactive case the minimum are somewhat lower and their displacement faster. The differences after five days are of about a quarter of a wave length (see in each picture the position of the centres on the other one) and of 5 to 10 millibars. There then arises the question of whether it is worth spending computer time for something which will be useful perhaps only in a small number of situations; but of course it is very easy to answer that these cases are the ones the users are most interested in. All this means that the scheme must be able to work appropriately in all possible situations, regardless of the chances they have to occur, rather than having a good accuracy for some idealised situations and using a schematic systemisation of the input for adaptation. Once again we find the notion of generality or, in other words, we have to allow in the model a maximum of feedback processes governed by a minimum of free parameters without overestimation of the input information.

All of this, however, is only necessary if the output of the scheme can be used in a context which gives it its maximum efficiency: for example, a diurnal cycle without a boundary layer formulation where the exchange depends on stability would be a waste.

1.5 A proposal for the ECMWF radiation scheme

As a conclusion to this chapter we can quickly consider the input-output scheme of our radiation code which will soon be part of a new physical package and which will be tested against the GFDL one.

Figure 5 Walker, 1977

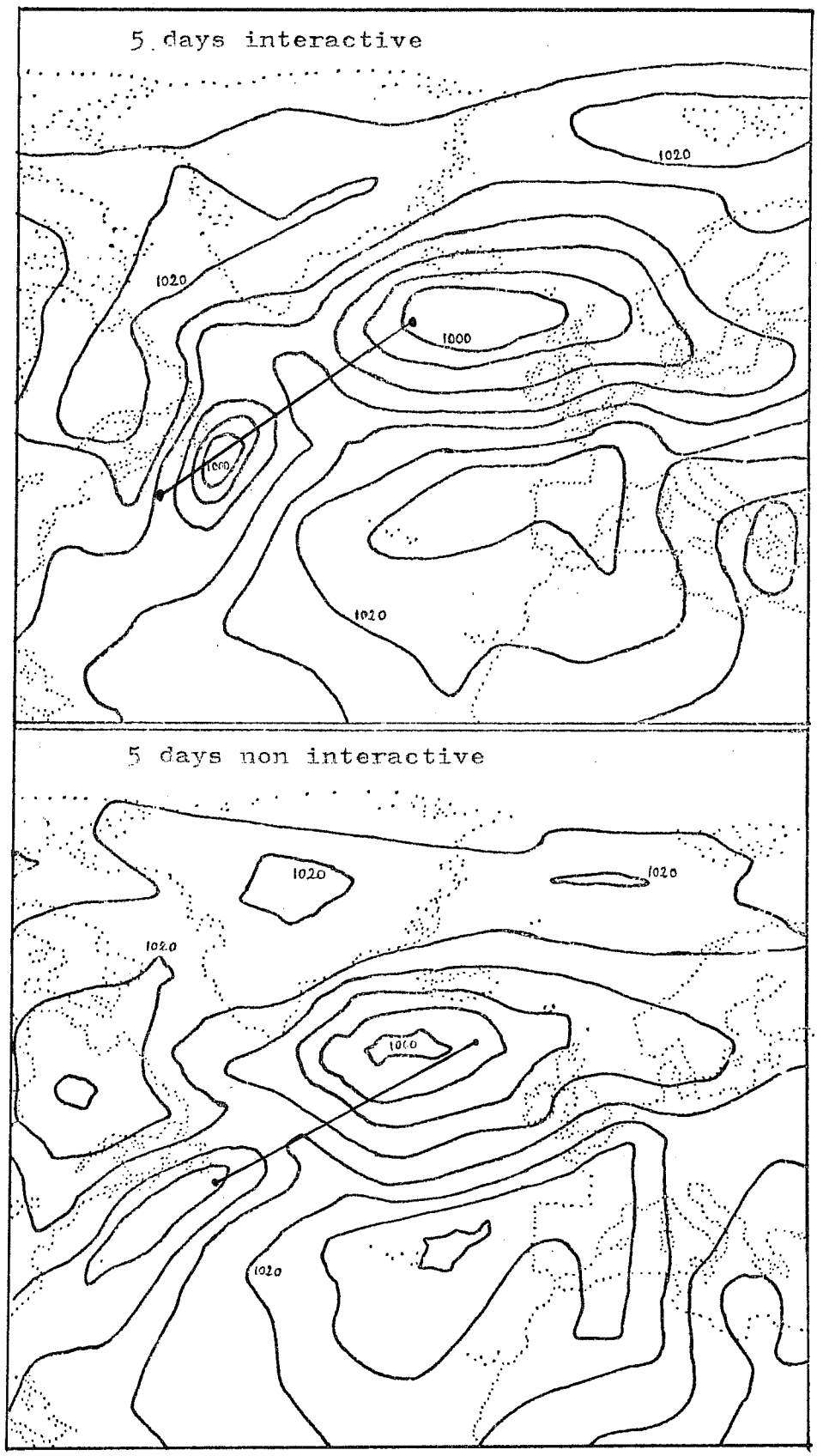

To compute radiation fluxes at the $\dot{\sigma}$ levels from infinity to the soil, we need the temperatures and pressures at the same levels and the mixing ratios of carbon dioxide, ozone, water vapour, saturation water vapour, liquid water and a characteristic of the aerosol importance as well as the cloudiness in the layers between these levels. The temperature at the soil will be constant on oceans and the result of a prognostic equation on continents, the intermediate temperatures will be interpolated between the prognostic levels in a way which has still to be decided and it remains the problem at infinity. With only one moisture prognostic variable in the global model, the mixing ratios of both liquid water and water vapour and the cloudiness will be related by diagnostic relationships, but it is still necessary to distinguish between clouds and the outside in the radiation code. Other necessary input parameters are the long wave and short wave albedos of the earth surface, the solar irradiance (function of the sun-earth distance) and the cosine of the solar zenith angle, which we can compute from latitude-longitude and time. The solar albedo of the soil will depend on soil moisutre and on snow height and, since there are few reliable global measurements for the thermal one, some relationship between both will be probably first assumed.

The computed fluxes will be used as usual through their divergences for the prognostic equation of atmospheric temperature and on continents the surface flux will be an element for the computation of surface temperature. The intermediate steps from the input to this output will be the subject of the next chapter of this lecture.

2. Proposed parameterization of radiation for medium range forecasts

2.1 Introduction

This second chapter aims to describe and justify the radiation parameterisation work which has been carried out for one year at ECMWF to get an alternative to the GFDL radiation package. As described in the preceding chapter, some specific needs of the medium range forecasting were taken into account and, looking ahead to the period of testing which has now started, the first version of the code was written in a very general form to allow flexible use.

The main difficulty in describing one's own work is the choice of the explanation method. One can either choose the historical way and go through the diverse stages of the development, or take the result of this process and explain it globally, starting from basic theories or compare it with a well known similar work. The first method may be the most interesting one for the listener for its "life" aspect, but it is very difficult for the lecturer to remain objective while describing his choices without some explanation of the rejected solutions; however, it would have required more time than this part of the seminar is worth and we rejected it. The third method is the easiest one for the lecturer and it would have been a good introduction to our last chapter to systematically describe the differences between our scheme and the GFDL one, but some listeners may not be aware of the characteristics of the latter and we have therefore chosen the second solution.

In doing so we must often refer to basic radiation theories and the best and closest reference the reader can take is the lecture given by Dr. C. Rodgers at this seminar, which we simply refer to as RODGERS. We first write again the radiative equation of transfer and then explain the few simple hypotheses whose application to this equation allows a rather simple solution of the three integration problems involved in its solution, and this without any loss of generality.

Before referring in the next chapter to the influence of radiation on dynamics, with some results of our scheme, we present here four kinds of simple basic experiments: test of reliability and sensitivity with a generation of numerous random atmospheres, radiative equilibrium experiments and comparison of the results with those of the Manabe-Möller (1961) paper, parallel with other schemes in test cases and finally comparison with measurements of the scheme, used either alone or coupled with a boundary layer model.

All these results were quite satisfactory, but the real test of the quality of our scheme has just started: by experimentations in the framework for which it has been designed and the first results will be presented in the next chapter.

2.2 The monochromatic equation of radiative transfer

At a given frequency ν we can write

$$\mu . \frac{\partial I_\nu(t_\nu,\mu,\phi)}{\partial t_\nu} = I_\nu(t_\nu,\mu,\phi) - \frac{1-k_\nu(t_\nu)}{4\pi} . \left[S_{o\nu} . e^{-t_\nu/\mu_o} . P_\nu(t_\nu,(\mu,\phi,-\mu_o,\phi_o)) + \int_0^{2\pi}\int_{-1}^{+1} P_\nu(t_\nu,(\mu,\phi,\mu',\phi')) . I_\nu(t_\nu,\mu',\phi') . d\mu' . d\phi' \right] - k_\nu(t_\nu) . B_\nu(T(t_\nu)) \quad (1)$$

with I_ν : intensity of the diffuse radiation

$S_{o\nu}$: intensity of the solar parallel radiation at the top of the atmosphere. The multiplication by e^{-t_ν/μ_o} gives us the local intensity as solution of the equation for parallel radiation: $-\mu_o \cdot \frac{dS_\nu(t_\nu)}{dt_\nu} = S_\nu(t_\nu)$

t_ν : optical thickness of the atmosphere used as vertical coordinate : 0 at the top and increasing downward

μ : cosine of the angle between the direction of radiation and the upward directed vertical

ϕ : azimuth angle of the direction of radiation

$-\mu_o, \phi_o$: μ and ϕ for the solar parallel radiation

k_ν : ratio of absorption to extinction (absorption plus scattering)

P_ν : scattering phase function normalised to the mean value 1 and with axial symmetry:

$$P(\mu,\phi,\mu'\phi') = P(\mu.\mu' + \sqrt{(1-\mu^2).(1-\mu'^2)}.\cos(\mu-\mu')) = P(\cos\theta)$$

B_ν : Planck function

T : Temperature

The four terms on the right hand side of (1) represent respectively

- The loss of energy by absorption and scattering
- The gain of energy coming from the scattered solar parallel radiation
- The gain of energy coming from the scattering of radiation from other directions
- The gain of energy through thermal emission

Supposing we know the vertical profiles of t_ν, T, k_ν and $P_\nu(\cos\theta)$ and the boundary condition for I_ν at the bottom of the atmosphere (at the top $S_{o\nu}\mu_o\phi_o$ are only dependent on geography and time) we can compute I_ν everywhere and therefore the spectral upward net flux is

$$F_\nu(t_\nu) = \int_0^{2\pi}\int_{-1}^{+1} I_\nu(t_\nu,\mu,\phi).\mu.d\mu.d\phi - \mu_o.S_{o\nu}.e^{-t_\nu/\mu_o} \qquad (2)$$

A spectral integration allows us to compute our final goal: the net upward radiation flux

$$F(p) = \int_o^\infty F_\nu(t_\nu(p))d\nu \qquad (3)$$

with p pressure as vertical coordinate

The signification of all the previous equations and definitions is more or less intuitive. For more complete information refer to Rodgers.

The exact solution of the radiative transfer equation involves three types of integration: over angles, over the vertical coordinate and over the wave length spectrum. We shall describe here successively the way of solving the three problems arising from these integrations.

2.3 The spectral integration problem

We first suppose that we can separate the whole spectrum into two intervals: the long waves where we put $S_{o\nu} = 0$ and the short waves with $B_\nu(T) \equiv 0$. Because of the difference between the radiative temperatures of the sun (5750^oK) and of the earth (254^oK) this simplification is very reliable.

Let us then suppose that we are able to do the necessary computations to solve the monochromatic problem in both spectral ranges. In order to avoid a great number of such computations at different frequencies we have to find how to determine and use t, k and $P(\cos\theta)$ representative for wide parts of the spectrum.

The solution of the monochromatic equation being of negative exponential type (as we shall see later on), the main problem comes from the highly non-linear nature of the exponential operator: ($e^{-\frac{a+b}{2}} \neq \frac{e^{-a}+e^{-b}}{2}$ a strong and a weak extinction cannot be combined in an intermediate one): the use of spectrally averaged coefficients of absorption and scattering is only valid when the real coefficients have the same order of magnitude throughout the considered spectral interval.

We suppose that this is the case for cloud-aerosols absorption and scattering (less than one order of magnitude variation for the extinction coefficients) and Rayleigh scattering (only present in short waves) in a small number of domains (3 for long waves, 2 for short waves) and we have grey effects except for gaseous absorption in these intervals.

The experimental data were taken from ZDUNKOWSKI, KORB and NIELSEN (1967).

The aerosols are included in the scheme more to give a possibility of fitting the results of the model and to smooth the transition between cloudy and non-cloudy conditions than to represent the poorly known effect of natural aerosols (the dynamical model does not give their geographical distribution and their optical properties are uncertain).

There is first a dry effect proportional to the quantity of aerosols (given climatologically and idealised) with a constant absorption coefficient throughout the whole spectrum and a scattering coefficient increasing the Rayleigh effect and modifying its phase function in short waves. Furthermore, outside of the clouds, we assume empirically an adsorption of water proportional to the quantity of aerosols and to U/(1-U) (U being the relative humidity). The optical properties of this smog are the same as those of clouds. We hope that the use of averaged coefficients for cloud and aerosols will not create a bigger error than the error caused by the poor knowledge that we have from their optical properties themselves.

The Rayleigh effect, although highly non-linear (coefficients proportional to ν^4) is sufficiently small so that we can choose empirical coefficients for which the effect of the first scattering is well parameterised (by taking into account the zenith angle of the sun) without having important errors for the subsequent scatterings.

An extra difficulty arises in the case of gaseous absorption, the coefficients depending strongly on temperature and pressure. (There is also a temperature dependence for the other effects in the long wave domains, due to the change of shape of the Planck function with temperature. However, it can be well parameterized by a linear dependence of the spectral coefficients on the inverse of temperature). For the gases, their line-type absorption spectrum obviously makes the averaging of coefficients hopeless, since strong absorption and no absorption at all are present together in the same parts of the spectrum.

We must therefore use empirical transmission functions for the gases. The theory of gaseous absorption (refer to Rodgers) shows that these transmission functions can be expressed over some spectral intervals as the product

of the individual transmission functions for the different gases; but we can group the effect of all the gases which have a constant mixing ratio throughout the atmosphere as if it would be the effect of the most important of them: CO_2. So we have only three gases to consider: water vapour, ozone and carbon dioxide.

Furthermore, we shall use for each of them the two parameters scaling approximation (Curtis Godson approximation): the transmission function is expressed in terms of the unreduced amount of absorber $u = \int r dp$ (r being the mixing ratio of the gas) and of the reduced amount $u_r = \int rp/\sqrt{T}\, dp$. (The dimensions of u and u_r does not matter; the product with absorption coefficients has only to be dimensionless).

For a narrow spectral range one can compute the transmission τ from

$$-\ln \tau = \frac{au}{\sqrt{1+bu^2/u_r}} + cu_r \qquad \text{(see RODGERS)} \qquad (4)$$

The term cu_r represents the absorption of the continuum; for weak absorption the first term on the right hand side of (4) becomes au and for strong absorption $a\sqrt{u_r/b}$. These two formulations are the ones given by the theory of band absorption. The coefficients a, b and c depend on temperature.

By analogy to this form we choose an empirical transmission for the five spectral domains or for sub-intervals of them as

$$\tau = \prod_{H_2O,\ CO_2,\ O_3} \left(\frac{1}{1+\frac{au}{\sqrt{1+bu^2/u_r}}+cu_r} \right) = \tau_T(u_{H_2O}, u_{rH_2O}, u_{CO_2}, u_{rCO_2}, u_{O_3}, u_{rO_3})$$

a, b, c depending linearly on 1/T are fitted to experimental data.

But to use these transmission functions we need to know the encountered unreduced and reduced amounts of H_2O, CO_2 and O_3 along the different radiation paths. We can reduce our search to the evaluation of the mean value for each of these 6 amounts and introduce them in the transmission functions. Since these are still non linear we make there an error but a smaller one than by averaging the coefficients a priori.

Let us see in detail this evaluation in the case of short wave radiation. We first make a monochromatic computation without any gaseous absorption, the resulting flux at the reference level being F_o; the way this result is obtained will be shown in part 4. F_o can represent either the solar parallel flux or the upward or the downward diffuse flux. Now we add each gas (H_2O, CO_2 and O_3) in both reduced and unreduced amounts (6 cases) with an arbitrary but very small absorption coefficient k_i; the

the intensities replaced by the fluxes (explanation in Appendix A).

2.4 The vertical integration problem

Following the principle expressed in the previous chapter we do not try to extract more information from the input parameters than they can give us. Therefore, we suppose that each layer is a vertically homogeneous absorbing and scattering medium and as an interpolation assumption that in each spectral interval of the long wave domain the Planck functions vary linearly with the optical thicknesses through every layer.

We make now the so-called Two-stream Eddington approximation. At each level both upward and downward diffuse radiation fields are hemispherically isotropic (I depends only on the sign of μ).

We can now compute a matrix solution of the radiative transfer equation for each layer: the outgoing fluxes depend linearly on the incoming ones and (in the long wave domain) on the black body fluxes at the boundaries.

$$\begin{bmatrix} S_b \\ F_{1t} \\ F_{2b} \end{bmatrix} = \begin{bmatrix} a_1 & o & o \\ a_2 & a_4 & a_6 \\ a_3 & a_5 & a_7 \end{bmatrix} \cdot \begin{bmatrix} S_t \\ F_{1b} \\ F_{2t} \end{bmatrix} \qquad (9)$$

t for top b for bottom

S solar parallel flux

F_1 solar upward diffuse flux

F_2 " downward " "

and

$$\begin{bmatrix} F_{1t} \\ F_{2b} \end{bmatrix} = \begin{bmatrix} b_1 & b_3 \\ b_2 & b_4 \end{bmatrix} \cdot \begin{bmatrix} F_{1b} \\ F_{2t} \end{bmatrix} + \begin{bmatrix} b_5 & b_7 \\ b_6 & b_8 \end{bmatrix} \cdot \begin{bmatrix} \pi B_b \\ \pi B_t \end{bmatrix} \qquad (10)$$

F_1 thermal upward flux

F_2 " downward "

See appendix A for the computation of the a and b coefficients:

The b coefficients are functions of - the optical thickness of the layer Δt

- the ratio absorption/extinction k
- an integral factor of the phase function:

$$A_1 = \int_0^{2\pi}\int_0^1\int_0^{2\pi}\int_0^1 \frac{\underline{P}(\mu,\phi,\mu',\phi')}{8\pi^2} d\mu d\phi d\mu' d\phi'$$

result is F_i. We can say that the mean encountered amount of this absorber type u_i is given by $u_i = \frac{1}{k_i} \cdot \frac{Fo-Fi}{F_i}$ (5)
(From $F_i = F_o e^{-k_i u_i} \simeq F_o/(1 + k_i u_i)$). Finally we compute the real flux with $F = F_o.\tau(u_i, i = 1,6)$.

In the long wave part of the spectrum the problem is more complicated. There is not a single external source but every absorption is accompanied by an equivalent emission depending on temperature through the Planck function. Hence to evaluate the amounts of absorbers we have to compare runs with and without gases in an isothermal case (only the optical thickness matters, not the Planck function which is B* throughout the atmosphere). We get the fluxes (see part 4 again) F_o^* and F_i^* (either upward or downward diffuse fluxes)

u^*_i is given by $u^*_i = \frac{1}{k_i} \cdot \frac{F_o^*-F_i^*}{F_i^*-\pi B^*}$ (6)

(From $F_i^*-\pi B^* = (F_o^*-\pi B^*).e^{-k_i u_i} \simeq \frac{F_o^*-\pi B^*}{1+k_i u_i}$)

and we get $\tau^*(u^*_i, i = 1,6)$

The ratio $F^*_o/\pi B^*$ is the emissivity ε^* in the isothermal case without absorber.

We need then to compute the flux F_o in the case without absorber but with the actual temperature state of the atmosphere. There B_r is the Planck function in the reference level.

Finally we compute the real flux F by making an analogy to the short waves. We had there F as the result of the transmission without scattering of F_o through a layer of transmissivity τ. Here F is the result of the transmission through a layer of transmissivity $\tau = \tau^*$ with, at the origin, a flux F_o provided by an emission with emissivity $\varepsilon = \varepsilon^*$. For the computation we suppose, as we shall do in each case, that the Planck function varies linearly with the optical thickness taken as vertical coordinate: $t = -\ell n\tau^*$. We obtain

$$F = \pi B_r+(F_o-F_o/\varepsilon^*).\tau^*+(F_o/\varepsilon^*-\pi B_r).(\tau^*-1)/\ell n\tau^* \quad (7)$$

when we integrate the simplified version of (1).

$$\frac{dF}{dt} = F-\pi B = F-\pi(B_o+B't) \quad (8)$$

in which the scattering effects have been suppressed and

The a coefficients are functions of the same parameters and of

- the cosine of the solar zenith angle μ_o
- a second integral factor of the phase function depending on μ_o:

$$A_3(\mu_o) = \int_o^{2\pi} \int_o^1 \frac{\underline{P}(\underline{\mu}, \underline{\phi}, -\mu_o, \phi_o)}{4\pi} \, d\mu d\phi$$

To compute the mean encountered amounts of gaseous absorbers we should recompute 6 times the a and b coefficients. Since the changes in optical thicknesses $k_i . u_i$ are arbitrarily small we can avoid this amount of new computations if we take analytically the derivative a' and b' of the coefficients a and b with respect to the absorption optical thickness ($k\Delta t$) under the condition $(1-k)\Delta t$ constant.

The new a and b are given by $a + a' k_i u_i$ and $b + b' k_i u_i$

See appendix B for the computations of the a' and b' coefficients.

Each layer is thus characterised in each spectral interval by 30 coefficients.

A little supplementary treatment is needed when we have a cloudy layer with partial coverage. We compute the a and b coefficients for both cloudy and clear parts. Then we distinguish two cases. If the layer is alone between two clear sky layers, we simply do a linear combination of the coefficients with the amount of cloudiness and its complement to 1 as weights.

If there are several adjacent cloudy layers, building a so-called "cloud" we compute the coefficients which, if the layers were homogeneous would give the same results as those obtained in the following way: we suppose that the overlapping of the adjacent cloudy parts is maximal, and so we have n + 1 vertical distributions of cloudy and non-cloudy parts (n number of layer in the cloud); we compute the results inside the "cloud" for each combination for arbitrary incoming fluxes and finally combine linearly the results with the weights given by the geometry of the "cloud" and eliminate the arbitrary incoming fluxes from the equations. (See Appendix C)

When in each spectral interval, for each case (with and without gaseous absorption, isotherm or not) we have the a and b coefficients of each layer, we can compute all the fluxes through the atmosphere as resulting from a linear system. (An example can be seen in Appendix C).

For this we only need the boundary conditions which are for short wave fluxes:

- S_∞ given by astronomical considerations
- $F_{2\infty} = 0$
- $F_{1z=o} = A\ell \; F_{2z=o} + A'\ell(\mu o) S_{z=o}$

  $A\ell$ and $A'\ell$ ground albedos for diffuse and parallel radiation

and for long wave fluxes:

- $F_{2\infty} = 0$
- $F_{1z=o} = \varepsilon \pi B_{z=o} + (1-\varepsilon) F_{2z=o}$

  ε emissivity of the ground.

(We suppose for simplicity that $A\ell$, $A'\ell$ and ε are the same in the different spectral intervals).

2.5 The angle integration problem

As seen before, we make the hypothesis of hemispheric isotropy. Therefore we need a magnification factor for diffuse fluxes which multiplies the quantities of absorbing and scattering media computed for a vertical beam. For all effects except gaseous absorption we take this factor equal to 2. This value is the one for small effects as seen in Appendix A. We choose it because the involved effects are either small (outside of clouds) or strong (in the clouds) and then the fluxes do not depend on the quantities of acting media any longer. For gaseous absorption we have two different factors: 2 for the unreduced amount of gases and 25/16 for the reduced amounts. This later value is the one we obtain as a limit for transmission zero in the form $\tau = 1/(1+a\sqrt{u_r/b})$ (see part 3).

Thus our magnification factor diminishes with increasing absorption as it is the case in nature. The usually accepted value of 5/3 falls between our two values.

As all our computation of a and b coefficients are done with the magnification factor 2 we need to correct the quantities $k_i.u_i$ for reduced amounts of absorbers. We multiply them by a factor 25/32 for the linear computation of the coefficients $a_{4\ldots7}$ and $b_{1\ldots8}$. For the coefficient a_1 we have no modification to do since it concerns a parallel beam. For a_2

and a_3 we assume (only for this purpose) that there is only a single scattering taking place in the middle of the layer. On the way in we have a path length proportional to $1/\mu_o$ and a multiplying factor 1. On the way out the path length is proportional to 2 and the factor is 25/32. So our final factor is

$$(\frac{1}{\mu_o} \cdot (1) + 2 \cdot (\frac{25}{32}))/(\frac{1}{\mu_o} + 2)$$

2.6 First results of the model

It should first be noticed that the empirical transmission functions for gases used here are not yet definitive (there is no division in sub-intervals and we have still to introduce the self broadening effects) but they already give a good idea of the possibilities of the scheme. For the basic data which help us to determine these functions we use McCLATCHEY et al. (1973) and VIGROUX (1953).

There are two determinant assumptions in the model, the direct use of a multiple scattering method instead of an emissivity type (with mathematical separation of scattering and absorption as, for example, in the GFDL radiation scheme), and the simplification in the long waves $\varepsilon = \varepsilon^* \; \tau = \tau^*$ which is in a certain sense the equivalent in our formalism of the so-called "cooling to boundaries" approximation. (In the latter approximation, for the computation of the fluxes at a given reference level one assumes that the atmosphere is isothermal with the temperature of the reference level). (See Rodgers).

We will try here to justify these two choices by showing the influence they have on the results of the model for a great amount of possible atmospheric configurations. We apply our model to a set of 142 atmospheres (with 15 layers) whose characteristics of temperature, humidity and cloud coverage are randomly distributed around reasonable profiles (see Appendix D) with the help of the random number generator of the computer. The distribution of the solar zenith angle is also random between -1 and +1. The values for ozone and carbon dioxide do not vary and are taken from observations (McCLATCHEY et al. (1972)). The number of 142 is the one for which the averaged results have the best flux balance at the top of the atmosphere (net flux as small as possible) for a computing time less than 1 minute.

It is interesting to note that this is accompanied by a good cooling-heating balance at p = o too. This can be seen

on Fig. 1. In this figure we have computed the results of cooling-heating rates of the model (full lines) and of a modified version in which there is no more scattering of the diffuse radiation (A1 ≡ 1 in Appendix A), for long wave and short wave separately and for their sum. At the top and the bottom the net fluxes (in W/m^2) are indicated.

One can see that neglecting the multiple scattering leads to errors of the order of 25% for the divergences and of 50% for the fluxes (relative to the values of long wave or short wave fluxes before they cancel by summation). Although the errors are larger for short waves than for long waves, these latter are still important, particularly in the middle of the atmosphere where both differences are additive, whereas in the boundary layer (with more long wave cooling of the last layers without reflection of "warm" radiation from the upper levels) and in the stratosphere (with the short wave absorption by ozone of multiple-scattered radiation on its way back to space) they tend to cancel each other.

Considering only the results of the model for the net radiation we can see an important cooling in the boundary layer, an almost constant cooling rate throughout the troposphere, another increase of cooling (it will create the tropopause which does not exist in our data) at the bottom of the stratosphere, and finally, as already pointed out, an equilibrium at the top.

However, at p = 0 both long wave and short wave fluxes are too low (right value ≃ 237). This is probably due to the absence of a positive lapse rate of temperature in the stratosphere and to a too high liquid water content of the clouds.

For the second point mentioned above, there is no possibility in the framework of the code to see what would be the results with temperature dependent emissivity and transmissivity. However, it is possible to compute the changes in the fluxes for small k_i coefficients in the real temperature state of the atmosphere as we have done for the isothermal case (with the use of a' and b' coefficients). Therefore, we can compare these tendencies with the one predicted by the model when

$$\tau^* = \frac{1}{1 + k_i\, u_i} \quad \text{in equation (7).}$$

For the same set of 142 random atmospheres the correlation coefficient between the two sets of results is 0.838. This result might be improved by using real data where the temperature profiles are probably more regular than the one we get from the random generation. However, it seems already worth doing this hypothesis considering the amount of integral computation which is saved (instead of varying with the square of the number of levels, the amount of computation for long wave fluxes varies with this number itself).

Figure 1

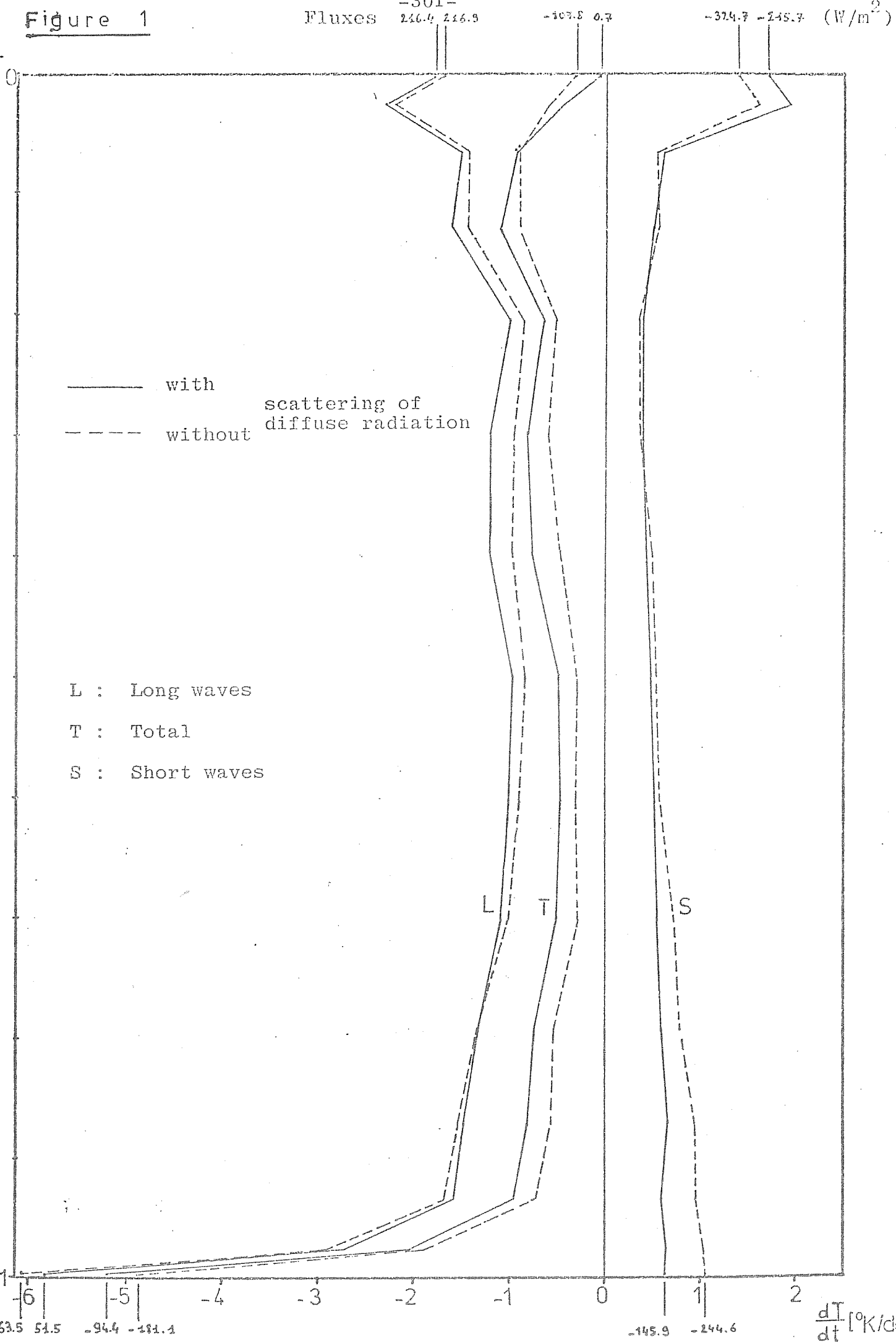
Fluxes
246.4 216.9
-109.8 0.7
-324.7 -245.7 (W/m²)
0
1
——— with scattering of diffuse radiation
– – – – without
L : Long waves
T : Total
S : Short waves
L
T
S
-6
-5
-4
-3
-2
-1
0
1
2
63.5 51.5 -94.4 -181.1
-145.9 -244.6
dT/dt [°K/day]

2.7 Comparison with the Manabe-Möller experiment

In order to compare our scheme with that used in the GFDL model, we recalculated the MANABE-MÖLLER (1961) experiment on radiative equilibrium. The results are shown on figures 2, 3 and 4, corresponding to figures 12, 14 and 15 of the original paper. There are two input elements in our scheme to which the results are quite sensitive and which are unknown to the M.M. model: the emissivity of the soil and the saturation humidity (for the aerosols). We took arbitrarily the second from the standard atmospheric temperatures and the first equal to 0.99.

The scheme used here is not exactly the one described in the paper, since we had to suppress the dependence of the coefficients on temperature: for very low temperatures, some of them become negative and even if we set them to zero, this creates a computational instability.

On Figure 2 we can see that both schemes agree well in the troposphere, but that the stratospheric results are totally different. Furthermore, our scheme shows a very strong boundary effect (which in some extreme cases can lead to an inversion). However, this is a consequence of the strong boundary cooling already noticed in Figure 1 and which is an observable feature (see for example GAMP and

Figure 2

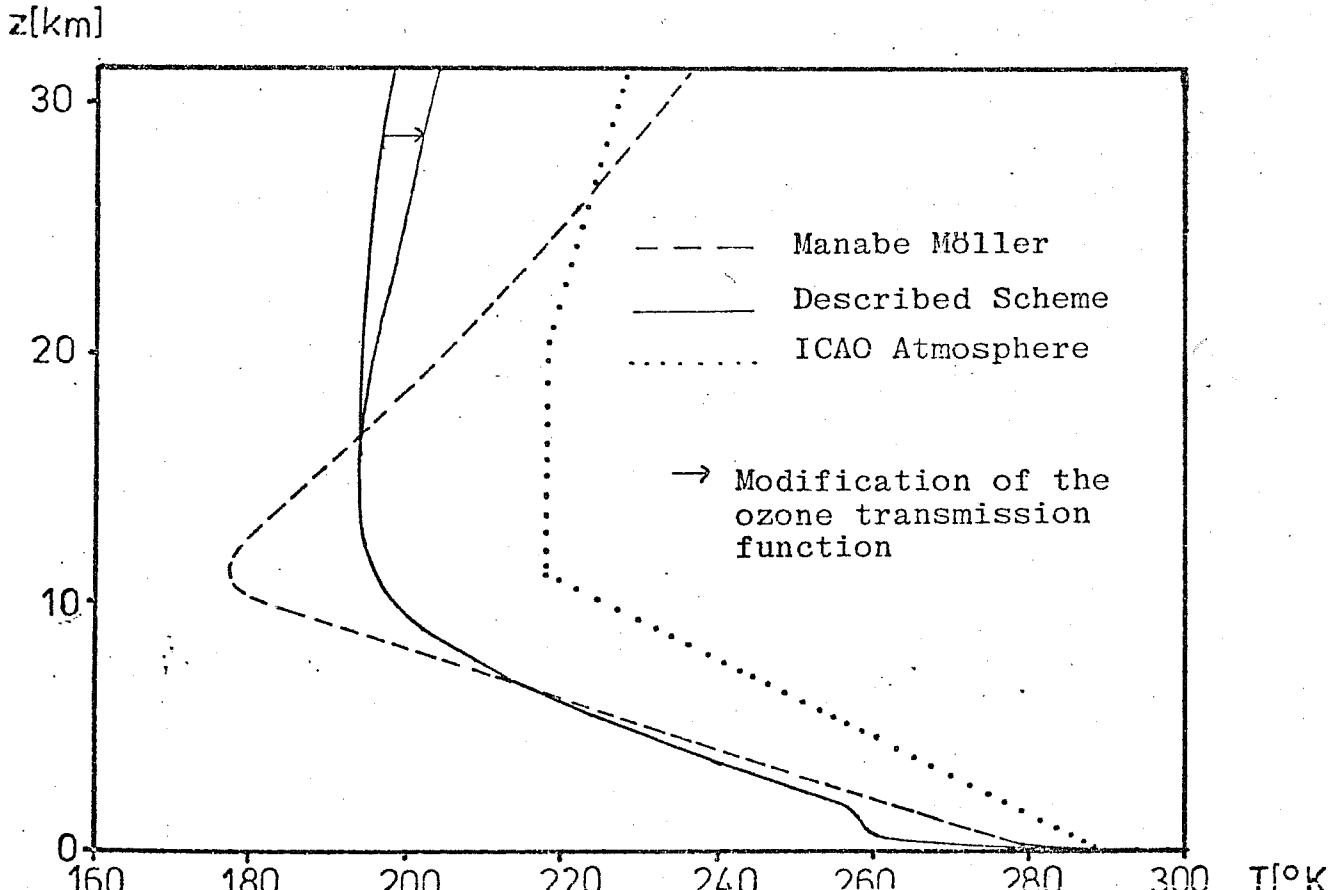

HEINRICH (1976). Thus we can already say that, if our scheme is to be used in a dynamical-physical model, this latter must have a treatment of the boundary layer, including the effect of stability in order to avoid the creation of too strongly unstable temperature gradients.

In Figures 3 and 4 we investigate the effect of a change only in the absorber quantities (3: ozone - 4: water vapour without change of the relative humidity) on the equilibrium conditions. The same remarks as for Figure 1 apply, but our scheme is more sensitive to water vapour and less sensitive to ozone than the M.M. one. The most important thing to notice is that the effect of the changes is more local in the M.M. case and spread throughout the atmosphere in our case. This will lead to a stronger computational stability in our scheme which is already proven by the fact that our critical time step for the computation of radiative equilibrium is about 8 to 16 times larger than the 12 hour time step given by M.M.

This difference of behaviour of the two schemes probably lies in their basic conceptions: - M.M.'s computes exactly what happens for a unique and a priori idealised photon path

- our scheme takes into account all photon paths but only

Figure 3

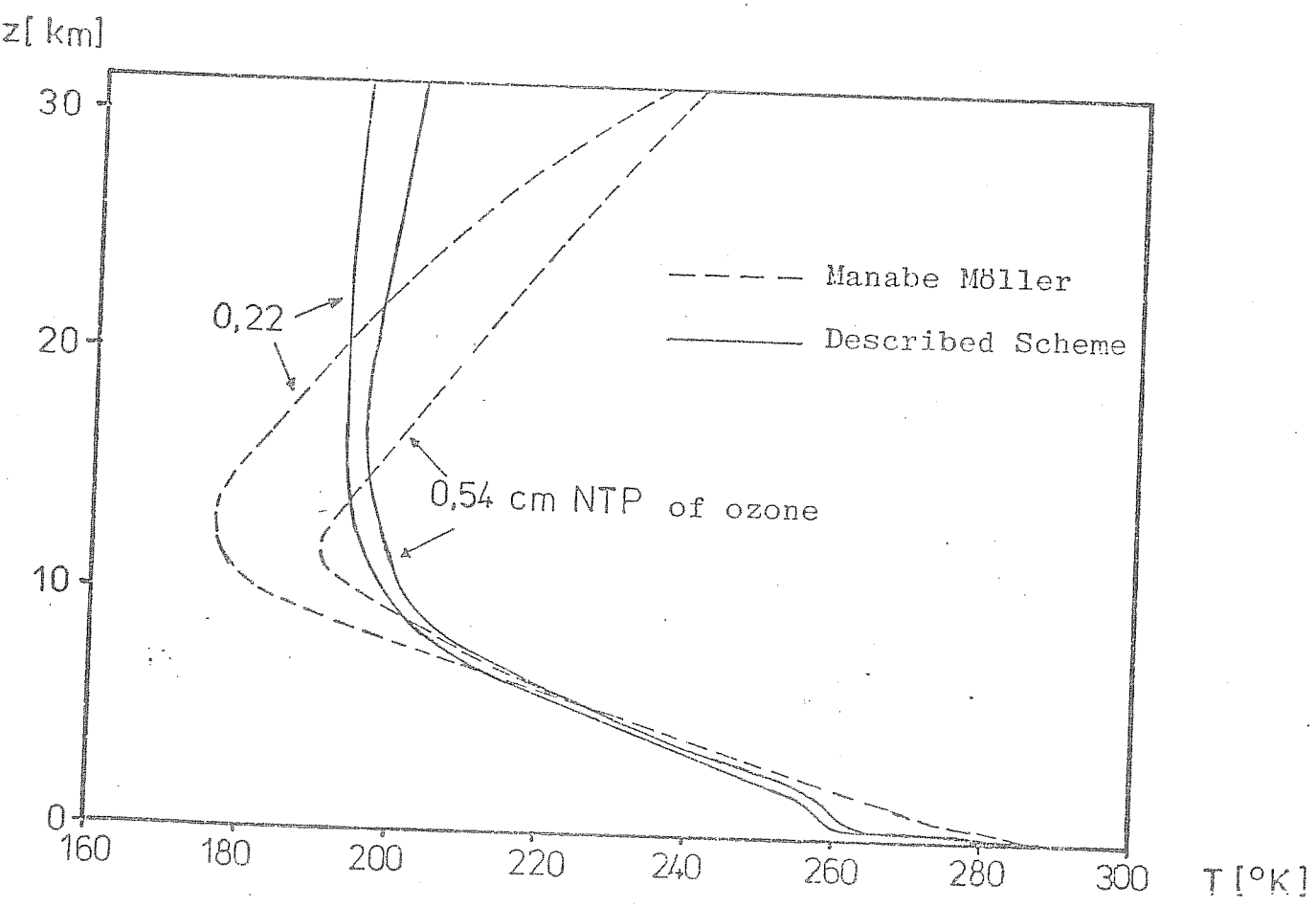

makes computation on averaged properties. Therefore every input parameter has an influence on every flux but strong local effects are somewhat smoothed by the averaging process.

The M.M. results have stratospheric values of temperature closer to the observed ones (represented in Figure 2 by the ICAO Standard Atmosphere), but our model has better lapse rates. Which of the two solutions is the more realistic is difficult to say, since the other physical effects will change the conditions of the equilibrium.

We can explain the discrepancies in the stratosphere with three reasons :

- our model does not separate the effects of the ultra violet and visible absorption bands of O_3 (it will later) and therefore our heating rates are too low above 25km. and too strong below. A test with a transmission function of a different type but taking into account both bands gives us an evaluation of the error (Figure 2).

Figure 4

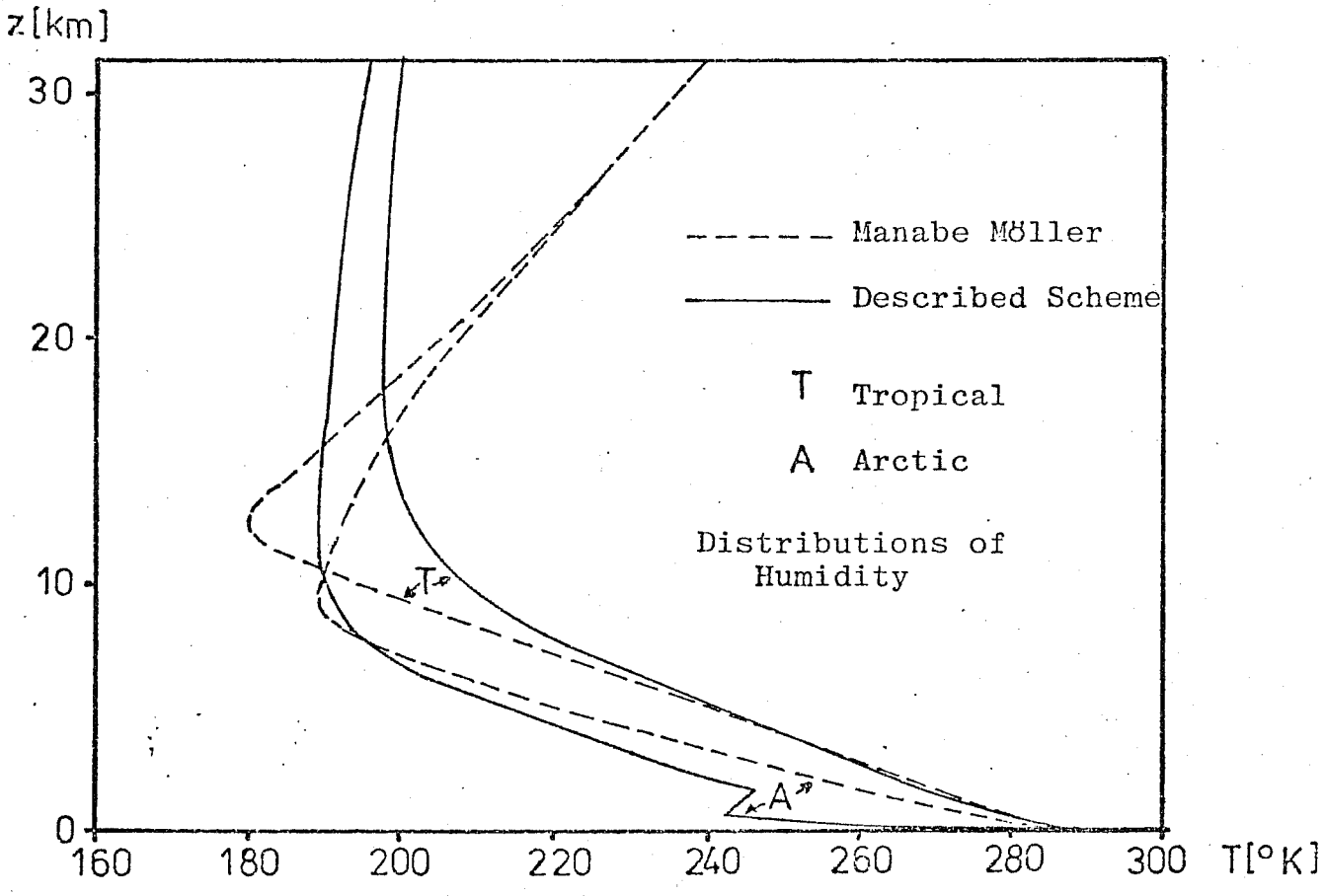

- The GFDL scheme has an upper boundary condition $dF/dp = 0$, which we cannot introduce in our computation since our temperatures are not at the same levels as theirs. (This feature also creates for us numerical problems for the computation of a convective-radiative equilibrium with a free soil temperature and this explains why we have to limit our present comparison to the first of the GFDL papers on equilibrium temperatures). In any case, in MANABE and STRICKLER (1964) with new transmission functions the stratospheric temperature and lapse rate are reduced in a slightly different experiment (free soil temperature as only change of conditions: Figure 1 of the M.S. paper).

- As already seen, the temperature effects are less local in our computations than in M.M.'s. This can also be seen if we compute a convective-radiative equilibrium with fixed soil temperature. The effect will not be a convective lapse rate extended until it reaches an unmodified radiative equilibrium, but rather a displacement of the whole stratospheric profile (See Figure 5).

Figure 5

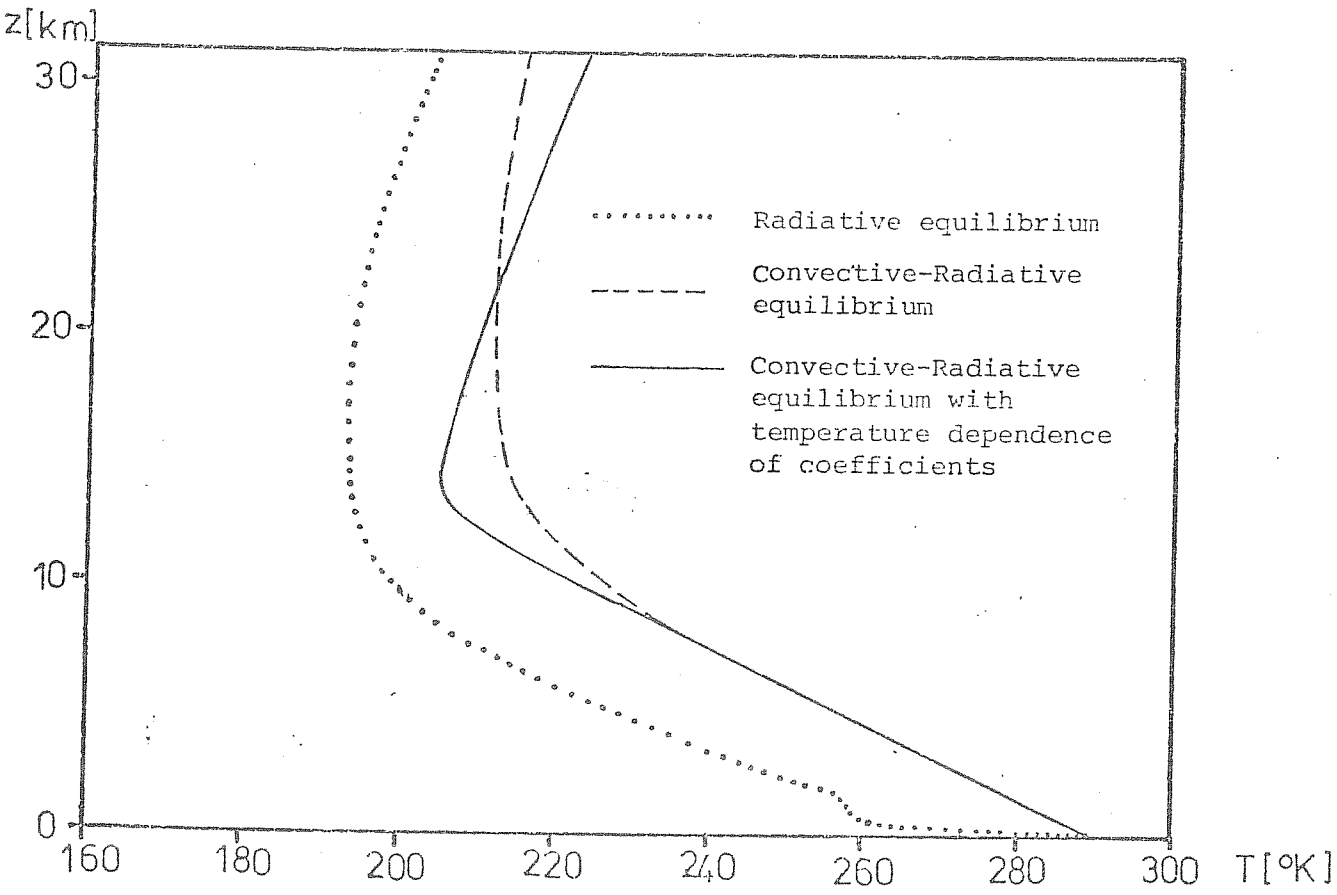

With these higher temperatures, however, we can return to our original model by reintroducing the dependence of coefficients on temperature. We then get a better stratospheric lapse rate and, for the first time, a well defined tropopause (see Figure 5 again in which all three curves are computed with the modified ozone transmission function).

2.8 Comparison with other schemes in test cases

This part of the work was not done at ECMWF but by BLONDIN (1977) using our model. The first set of experiments is a comparison of long wave cooling rates to the one computed by KATAYAMA in three situations with the same temperature profile but with different moisture repartitions. The results are shown on Figure C. Except between 600 and 700 mb., there is a very good similarity between the profiles although our

Figure 6

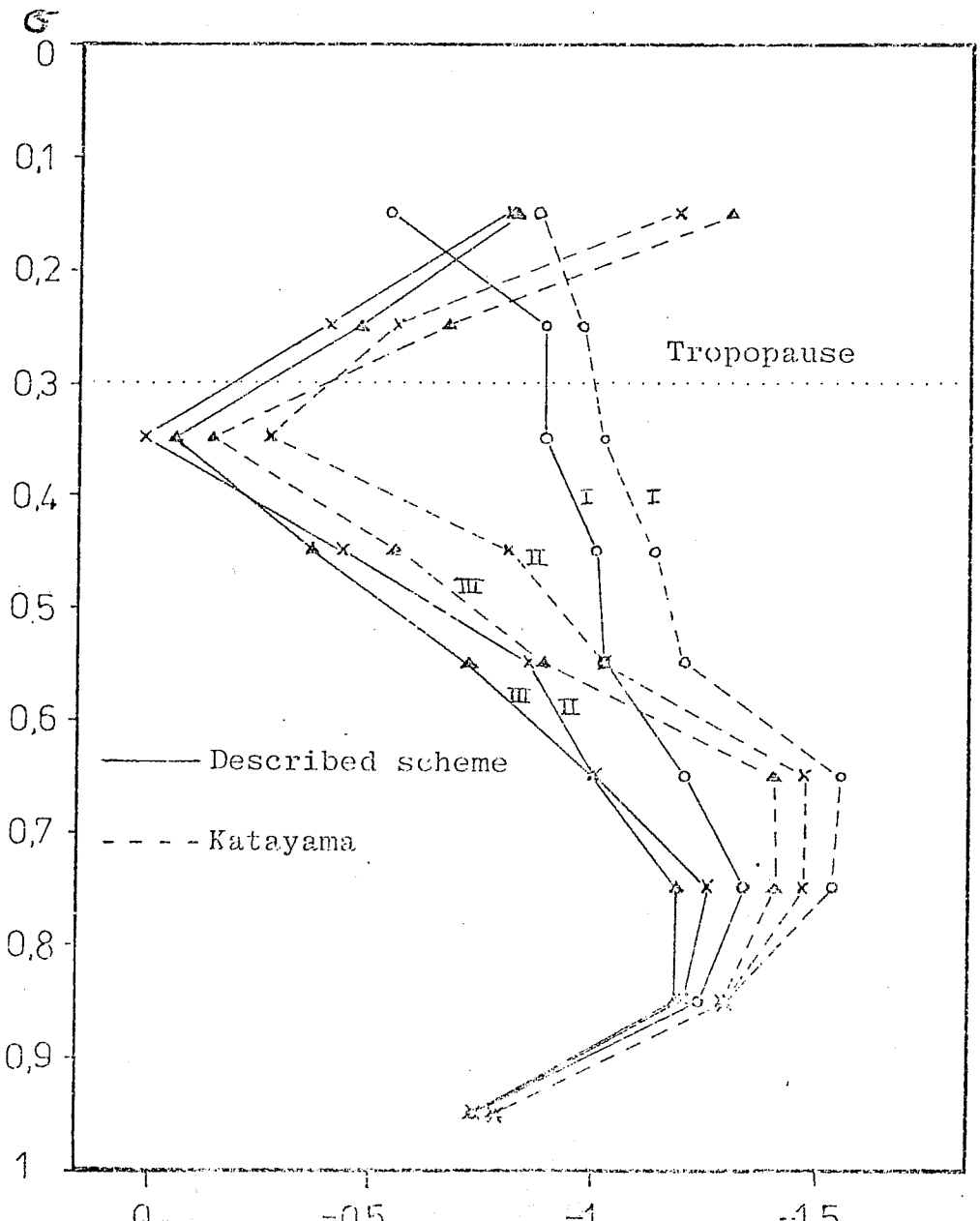

results are always somewhat smaller than those of KATAYAMA. The crossing point between curves I and III in our case is not at the tropopause but 100 mb. lower; this is the sign, as in paragraph G, of a different type of sensibility to changes in absorber quantities.

The second test case is the best known one for radiation studies: the tropical atmosphere of LONDON (1952). Our results for the long wave cooling are plotted against those of five other models: ELSASSER (1942), BROOKS (1950), YAMAMOTO (1952), YAMAMOTO and ONISHI (1953) and RODGERS and WALSHAW (1966). The same situation as in the previous example can be noticed for the upper atmosphere with too little cooling, but we have a far too high cooling rate in the lower troposphere which may be due to the inadequacy of our temporary transmission functions to great quantities of water vapour. The most interesting comparison is with the RODGERS-WALSHAW model which is the most comprehensive of all: although with different intensities we can find in our curve all the small scale features of the R-W one (see for example by 2, 9 and 13 km.). This proves that our

Figure 7

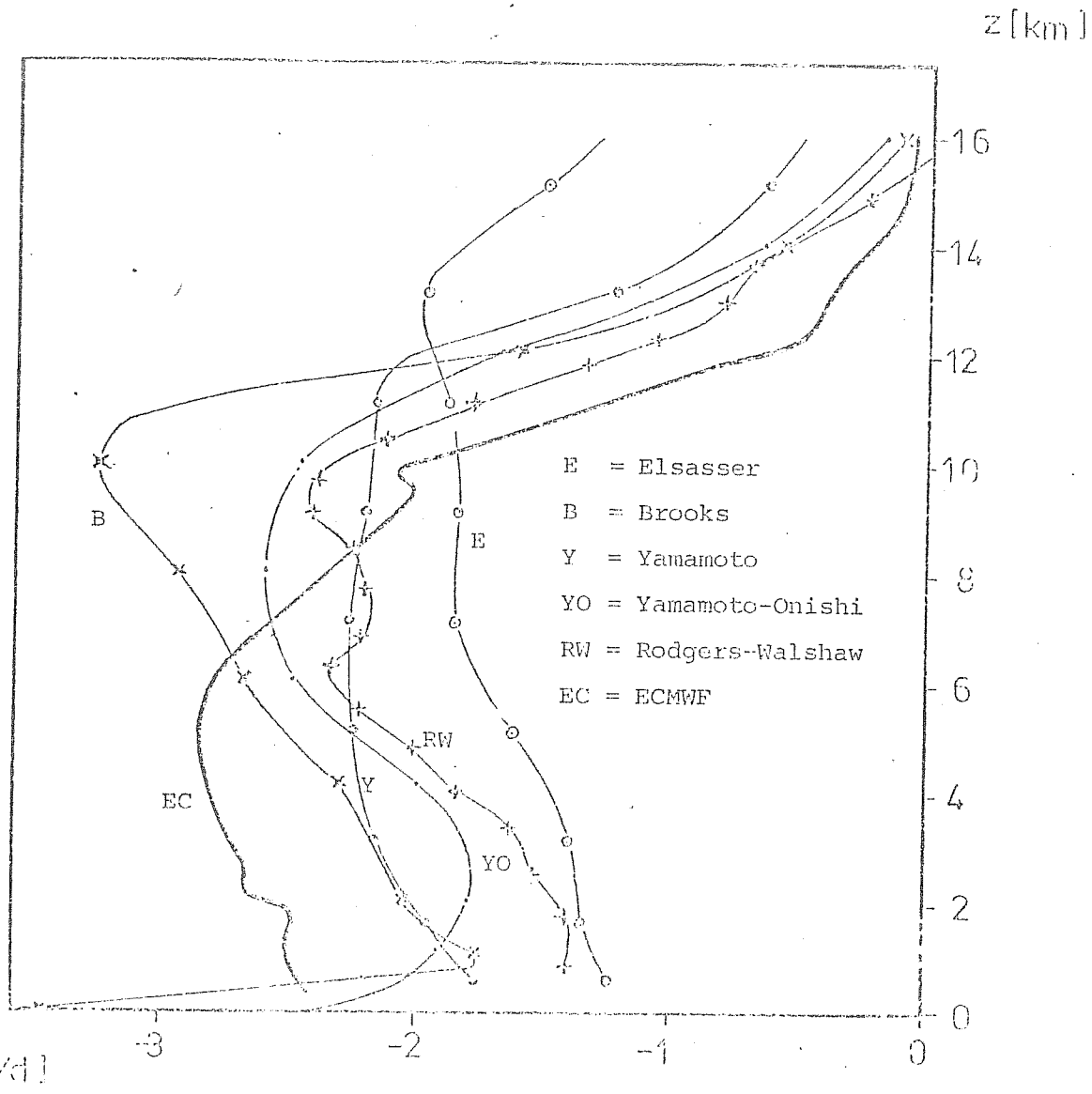

simplification for the vertical integration does not totally smooth out small scale phenomena and that our errors are more in the empirical transmission functions than in the way we use them.

2.9 Tests against direct measurements

We also tried our model against "real" situations, although it is very difficult to find a case for which a comparison can be significant: for one single experiment the measurements are not accurate enough and for a more comprehensive comparison all elements necessary to a simulation are seldom published. This is the case for the results shown in Figure 8 where we compare a mean of measured fluxes with the results of our computation from the mean state of temperature and specific humidity. The data are

Figure 8

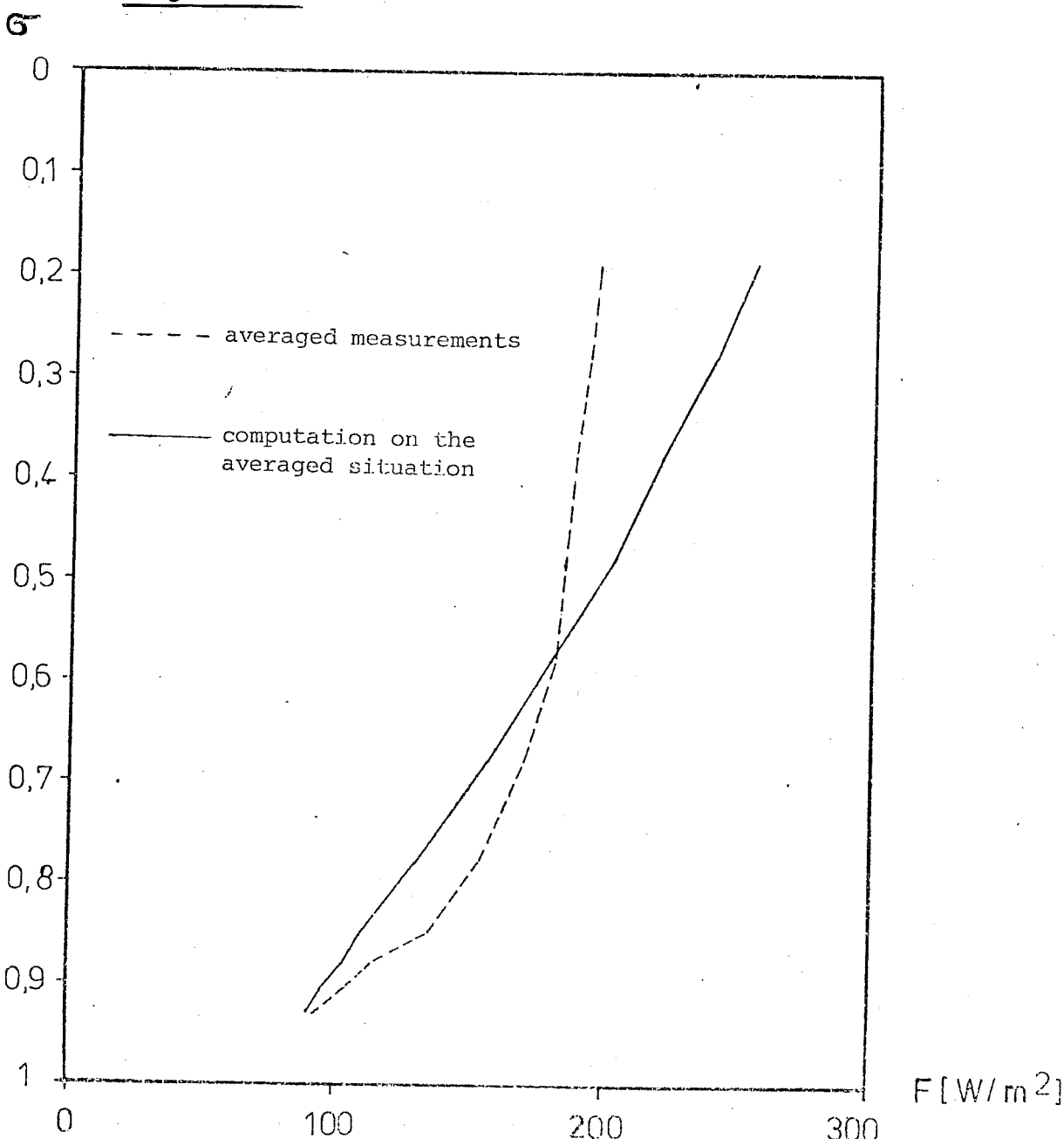

taken from KANO and MIYAUCHI (1977) and the fluxes are net long wave fluxes in cloudless cases. A test with our random generated atmospheres shows that the non linearity of radiation processes cannot account for the whole discrepancy seen here, which unfortunately is exactly the opposite of the one observed in Figure 7: we now have too little cooling in the lower part and too much in the upper part of the troposphere. Therefore some tests against other measurements will be needed to sort out this problem. The only positive point about this experiment is that the order of magnitude of the fluxes at the bottom of the atmosphere is right.

This is even more true for the last experiment we will present here. The planetary boundary layer parameterization proposed by J.-F. LOUIS (1977) and our radiation scheme were coupled to try and simulate the diurnal cycle observed in the O'Neill Nebraska experiment. Figure 9 shows a comparison of the computed net fluxes at the surface and of fluxes measured by two different experimental systems. Of course, most of the credit for the quality of the simulation is due to the PBL formulation but the good

Figure 9

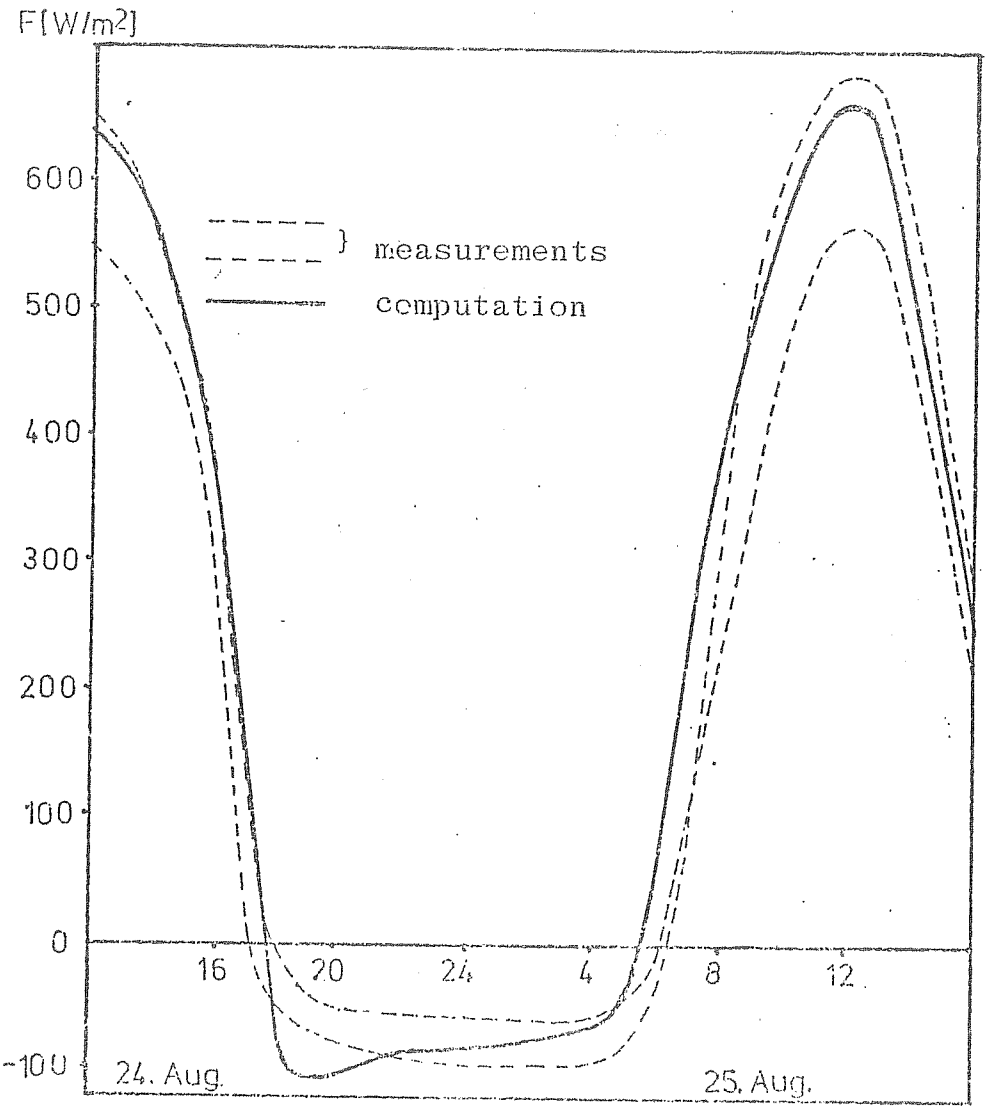

accuracy of fluxes at the ground was certainly helpful.

Of course, all comparative results presented here were for cloudless atmospheres, which is the most disadvantageous case for our scheme; but we could not find a reasonable case for testing our cloud inclusion in the scheme.

APPENDIX A

Calculation of the a and b coefficients introduced in 2.4

We consider one layer in which the optical thickness t varies from 0 at the top to T at the bottom, k and P (cosθ) are constant and B is linear in t.

We write the equation (1) in the form

$$\frac{\partial I(t,\mu,\phi)}{\partial t} = \frac{1}{\mu}\left[I(t,\mu,\phi) - \frac{1-k}{4\pi}\left\{I_o.P(\mu,\phi,-\mu_o,\phi_o) + \int_o^{2\pi}\int_{-1}^{+1} P(\mu,\phi,\mu',\phi').I(t,\mu',\phi').d\mu'.d\phi'\right\} - k.B(t)\right]$$

We suppose the radiation field hemispherically isotropic with I_1 (upward) and I_2 (downward) and we apply the operator $\int_o^{2\pi}\int_o^{+1} \mu.d\mu.d\phi$ to our equation:

$$\frac{dI_1(t)}{dt}.\int_o^{2\pi}\int_o^{1} \mu.d\mu.d\phi = I_1(t).\int_o^{2\pi}\int_o^{1} d\mu.d\phi - \frac{1-k}{4\pi}.I_o.$$

$$\int_o^{2\pi}\int_o^{1} P(\mu,\phi,-\mu_o,\phi_o).d\mu.d\phi - \frac{1-k}{4\pi}.I_1(t).\int_o^{2\pi}\int_o^{1}\int_o^{2\pi}\int_o^{1} P(\mu,\phi,\mu',\phi').$$

$$d\mu'.d\phi'.d\mu.d\phi - \frac{1-k}{4\pi}.I_2(t).\int_o^{2\pi}\int_o^{1}\int_o^{2\pi}\int_{-1}^{o} P(\mu,\phi,\mu',\phi').d\mu'.d\phi'.d\mu.d\phi$$

$$- k.B(t).\int_o^{2\pi}\int_o^{1} d\mu d\phi$$

But we have $F_1 = \int_o^{2\pi}\int_o^{1} I_1.\mu.d\mu.d\phi = \pi I_1 \qquad F_2 = \pi I_2$

Therefore

$$\frac{dF_1(t)}{dt} = F_1(t).\left[2 - \frac{1-k}{4\pi^2}.\int_o^{2\pi}\int_o^{1}\int_o^{2\pi}\int_o^{1} P(\mu,\phi,\mu',\phi').\right.$$

$$d\mu'.d\phi'.d\mu.d\phi\Big] - F_2(t).\left[\frac{1-k}{4\pi^2}.\int_0^{2\pi}\int_0^{1}\int_0^{2\pi}\int_{-1}^{0} P(\mu,\phi,\mu',\phi').d\mu'.d\phi'.d\mu.d\phi$$

$$- I_o(t).\left[\frac{1-k}{4\pi}.\int_0^{2\pi}\int_0^{1} P(\mu,\phi,-\mu_o,\phi_o)d\mu.d\phi\right] - 2k.\pi B(t)$$

Similarly with the operator $\int_0^{2\pi}\int_{-1}^{0} \mu.d\mu.d\phi$

$$\frac{dF_2(t)}{dt} = F_1(t).\left[\frac{1-k}{4\pi^2}.\int_0^{2\pi}\int_{-1}^{0}\int_0^{2\pi}\int_0^{1} P(\mu,\phi,\mu',\phi').d\mu'.d\phi'.d\mu.d\phi\right]$$

$$-F_2(t).\left[2 - \frac{1-k}{4\pi^2}.\int_0^{2\pi}\int_{-1}^{0}\int_0^{2\pi}\int_{-1}^{0} P(\mu,\phi,\mu',\phi').d\mu'.d\phi'.d\mu.d\phi\right]$$

$$+ I_o(t)\left[\frac{1-k}{4\pi}\int_0^{2\pi}\int_{-1}^{0} P(\mu,\phi,-\mu_o,\phi_o).d\mu.d\phi\right] + 2k\pi B(t)$$

But since $P(\mu,\phi,\mu',\phi') = P(\mu\mu'+\sqrt{(1-\mu^2)(1-\mu'^2)}.\cos(\phi-\phi'))$

$= P(-\mu,\phi,-\mu',\phi')$ we have

$$\int_0^{2\pi}\int_0^{1}\int_0^{2\pi}\int_0^{1} P(\mu,\phi,\mu',\phi')d\mu'.d\phi'.d\mu.d\phi = \int_0^{2\pi}\int_{-1}^{0}\int_0^{2\pi}\int_{-1}^{0} P(\mu,\phi,\mu',\phi').$$

$d\mu'.d\phi'.d\mu.d\phi$

On the other hand

$$\int_0^{2\pi}\int_0^{1}\int_0^{2\pi}\int_{-1}^{0} P(\mu,\phi,\mu',\phi')\ d\mu'.d\phi'.d\mu.d\phi = \int_0^{2\pi}\int_{-1}^{0}\int_0^{2\pi}\int_0^{1} P(\mu,\phi,\mu',\phi')$$

$d\mu'.d\phi'.d\mu.d\phi$

So we can write

$$\frac{dF_1(t)}{dt} = \alpha_1 F_1(t) - \alpha_2 F_2(t) - \alpha_3 I_o(t) - 2k\pi B(t)$$

$$\frac{dF_2(t)}{dt} = \alpha_2 F_1(t) - \alpha_1 F_2(t) + \alpha_4 I_o(t) + 2k\pi B(t)$$

Since $\int_o^{2\pi}\int_o^{1}\int_o^{2\pi}\int_o^{1} P(\mu,\phi,\mu',\phi').d\mu'.d\phi'.d\mu.d\phi + \int_o^{2\pi}\int_o^{1}\int_o^{2\pi}\int_{-1}^{o}$

$P(\mu,\phi,\mu',\phi').d\mu'.d\phi'.d\mu.d\phi = \int_o^{2\pi}\int_o^{1}\int_o^{2\pi}\int_{-1}^{+1} P(\mu,\phi,\mu',\phi').$

$d\mu'.d\phi'.d\mu.d\phi = \int_o^{2\pi}\int_o^{1} 4\pi d\mu d\phi = 8\pi^2$

and

$$\int_o^{2\pi}\int_o^{1} P(\mu,\phi,-\mu_o,\phi_o).d\mu.d\phi + \int_o^{2\pi}\int_{-1}^{o} P(\mu,\phi,-\mu_o,\phi_o).d\mu.d\phi =$$

$$\int_o^{2\pi}\int_{-1}^{1} P(\mu,\phi,-\mu_o,\phi_o).d\mu.d\phi = 4\pi$$

We get for the equations and the definition of their coefficients

$$\alpha_1 = 2(1 - (1 - k)A_1) \quad \alpha_2 = 2(1 - k)A_2 \text{ with } A_1 + A_2 = 1$$

$$\alpha_3 = (1 - k)A_3(\mu_o) \quad \alpha_4 = (1 - k)A_4(\mu_o) \text{ with } A_3(\mu_o) + A_4(\mu_o) \equiv 1$$

$$\frac{dF_1(t)}{dt} = \alpha_1(F_1(t) - \pi B(t)) - \alpha_2(F_2 - \pi B(t)) - \alpha_3 I_o(t)$$

$$\frac{dF_2(t)}{dt} = \alpha_2(F_1(t) - \pi B(t)) - \alpha_1(F_2 - \pi B(t)) + \alpha_4 I_o(t)$$

$$I_o(t) = I_o(0)e^{-t/\mu_o}$$

A. Long wave case

$$I_o \equiv 0 \qquad B(t) = B_o + B't$$

let us take $F_1^* = F_1 - \pi B \qquad F_2^* = F_2 - \pi B$

we have $\frac{dF_1^*(t)}{dt} = \alpha_1 F_1^*(t) - \alpha_2 F_2^*(t) - \pi B'$

$$\frac{dF_2^*(t)}{dt} = \alpha_2 F_1^*(t) - \alpha_1 F_1^*(t) - \pi B'$$

let us now take $F_1^{**} = F_1^* - \pi B'/(\alpha_1+\alpha_2); \quad F_2^{**} = F_2^* + \pi B'/(\alpha_1+\alpha_2)$

we get $\frac{dF_1^{**}(t)}{dt} = \alpha_1 F_1^{**}(t) - \alpha_2 F_2^{**}(t)$

$$\frac{dF_2^{**}(t)}{dt} = \alpha_2 F_1^{**}(t) - \alpha_1 F_2^{**}(t)$$

a) General case $\alpha_1 \neq \alpha_2$

We combine both equations in

$$\frac{d}{dt}(F_1^{**} - \beta F_2^{**}) = F_1^{**}(\alpha_1 - \beta\alpha_2) - F_2^{**}(\alpha_2 - \beta\alpha_1)$$

The homogeneous solutions are obtained for

$$\beta = \frac{\alpha_2 - \beta\alpha_1}{\alpha_1 - \beta\alpha_2} \qquad \beta^2\alpha_2 - 2\beta\alpha_1 + \alpha_2 = 0 \qquad \beta = \frac{\alpha_1 \pm \sqrt{\alpha_1^2 - \alpha_2^2}}{\alpha_2}$$

let us take $\varepsilon = \sqrt{\alpha_1^2 - \alpha_2^2} \qquad \beta_1 = \frac{\alpha_1 - \varepsilon}{\alpha_2} \qquad \beta_2 = \frac{\alpha_1 + \varepsilon}{\alpha_2} = 1/\beta_1$

We obtain $\frac{d}{dt}(F_1^{**} - \beta_1 F_2^{**}) = \varepsilon(F_1^{**} - \beta_1 F_2^{**}) \Rightarrow$

$$F_1^{**} - \beta_1 F_2^{**} = C_1 e^{\varepsilon t}$$

$$\frac{d}{dt}(F_1^{**} - \beta_2 F_2^{**}) = -\varepsilon (F_1^{**} - \beta_2 F_2^{**}) \Rightarrow$$

$$F_1^{**} - \beta_2 F_2^{**} = C_2 e^{-\varepsilon t}$$

$$F_1^{**} = (C_1 \beta_2 e^{\varepsilon t} - C_2 \beta_1 e^{-\varepsilon t}) / (\beta_2 - \beta_1)$$

$$F_2^{**} = (C_1 e^{\varepsilon t} - C_2 e^{-\varepsilon t}) / (\beta_2 - \beta_1)$$

With the boundary conditions

$$C_1 \beta_2 e^{\varepsilon T} - C_2 \beta_1 e^{-\varepsilon T} = (\beta_2 - \beta_1) F_1^{**}(T)$$

$$C_1 - C_2 = (\beta_2 - \beta_1) F_2^{**}(O)$$

Hence our equations are

$$F_1^{**}(O) = ((\beta_2 - \beta_1)F_1^{**}(T) + (e^{\varepsilon T} - e^{-\varepsilon T})F_2^{**}(O))/(\beta_2 e^{\varepsilon T} - \beta_1 e^{-\varepsilon T})$$

$$F_2^{**}(T) = ((e^{\varepsilon T} - e^{-\varepsilon T})F_1^{**}(T) + (\beta_2 - \beta_1)F_2^{**}(O))/(\beta_2 e^{\varepsilon T} - \beta_1 e^{-\varepsilon T})$$

Therefore

$$b_1 = b_4 = \tau_1 \cdot \frac{1 - \beta_1^2}{1 - (\beta_1 \tau_1)^2}$$

$$b_2 = b_3 = \beta_1 \cdot \frac{1 - \tau_1^2}{1 - (\beta_1 \tau_1)^2}$$

$$b_5 = b_8 = \frac{1 - b_1 + b_2}{(\alpha_1 + \alpha_2)T} - b_1$$

$$b_6 = b_7 = 1 - b_2 - \frac{1 - b_1 + b_2}{(\alpha_1 + \alpha_2)T}$$

$$\varepsilon = \sqrt{\alpha_1^2 - \alpha_2^2}$$

$$\beta_1 = (\alpha 1 - \varepsilon)/\alpha_2$$

$$\tau_1 = e^{-\varepsilon T}$$

b) Case without absorption

$$\alpha_1 = \alpha_2 = \alpha \iff k = o$$

$$\frac{dF_1^{**}}{dt} = \alpha(F_1^{**} - F_2^{**}) = \frac{dF_2^{**}}{dt} \Rightarrow F_1^{**} = F_2^{**} + C$$

With the boundary condition $C = F_1^{**}(T) - F_2^{**}(0) - C\alpha T$

$$F_1^{**}(0) = (F_1^{**}(T) + \alpha T.F_2^{**}(0))/(1+ \alpha T)$$

$$F_2^{**}(T) = (\alpha T.F_1^{**}(T) + F_2^{**}(0))/(1 + \alpha T)$$

therefore

$$b_1 = b_4 = 1/(1 + \alpha T)$$

$$b_2 = b_3 = \alpha T/(1 + \alpha T)$$

$$b_5 = b_6 = b_7 = b_8 = 0$$

B. Short wave case

$$B(t) \equiv 0$$

The parallel solar flux S is given by $S(t) = \mu_o . I_o(t)$

From the equation for parallel radiation $\boxed{a_1 = e^{-T/\mu_o}}$

and a_4, a_5, a_6, a_7 have the same expressions as b_1, b_2, b_3, b_4 since a diffuse radiation cannot become parallel again.

If S = 0 we have the same equation for F_1 and F_2 as in the longwave case for F_1^{**} and F_2^{**}

Let us try to derive the same expression valid for any S

$$F_1^{\odot} = F_1 - \gamma_1 S$$

$$F_2^{\odot} = F_2 - \gamma_2 S$$

$$\frac{dF_1^{\odot}}{dt} = \alpha_1 F_1^{\odot} - \alpha_2 F_2^{\odot} + I_o(\gamma_1 + \alpha_1\gamma_1\mu_o - \alpha_2\gamma_2\mu_o - \alpha_3)$$

$$\frac{dF_2^{\odot}}{dt} = \alpha_2 F_1^{\odot} - \alpha_1 F_2^{\odot} + I_o(\gamma_2 + \alpha_2\gamma_1\mu_o - \alpha_1\gamma_2\mu_o + \alpha_4)$$

We seek γ_1 and γ_2 so that $\gamma_1(1 + \alpha_1\mu_o) - \gamma_2\alpha_2\mu_o = \alpha_3$

$$\gamma_1\alpha_2\mu_o + \gamma_2(1 - \alpha_1\mu_o) = -\alpha_4$$

The discriminant of the system is $1 - \alpha_1^2\mu_o^2 + \alpha_2^2\mu_o^2 = 1-\varepsilon^2\mu_o^2$

a) General case $\varepsilon\mu_o \neq 1$

$$\gamma_1 = \frac{\alpha_3 - \mu_o(\alpha_1\alpha_3 + \alpha_2\alpha_4)}{1 - \varepsilon^2\mu_o^2} \qquad \gamma_2 = \frac{-\alpha_4 - \mu_o(\alpha_1\alpha_4 + \alpha_2\alpha_3)}{1 - \varepsilon^2\mu_o^2}$$

and

$$a_2 = -a_5\gamma_2 - a_4\gamma_1 a_1 + \gamma_1$$

$$a_3 = -a_4\gamma_2 - a_5\gamma_1 a_1 + \gamma_2 a_1$$

b) Resonance case $\varepsilon\mu_o = 1$

We no longer have a solution with γ_1 and γ_2 constants.

We seek now solutions with $\gamma_1 = \gamma_1^{o} + \gamma'_1(t/\mu_o)$

and $\gamma_2 = \gamma_2^{o} + \gamma'_2(t/\mu_o)$

The equations are now

$$(\gamma_1^{o} + \gamma'_1\frac{t}{\mu_o}).(1 + \alpha_1\mu_o) - (\gamma_2^{o} + \gamma'_2\frac{t}{\mu_o})\,\alpha_2\mu_o = \alpha_3 + \gamma'_1$$

$$(\gamma_1^{o} + \gamma'_1\frac{t}{\mu_o}).\alpha_2\mu_o + (\gamma_2^{o} + \gamma'_2\frac{t}{\mu_o})\,(1 - \alpha_1\mu_o) = -\alpha_4 + \gamma'_2$$

$$\frac{\gamma'_1}{\gamma'_2} = \frac{\alpha_2\mu_o}{1+\alpha_1\mu_o} = \frac{1 - \alpha_1\mu_o}{-\alpha_2\mu_o} = \frac{-\alpha_4 + \gamma'_2}{\alpha_3 + \gamma'_1}$$

We obtain

$$\gamma'_1 = \frac{-\alpha_3 + \mu_o(\alpha_1\alpha_3 + \alpha_2\alpha_4)}{2}$$

$$\gamma'_2 = \frac{\alpha_4 + \mu_o(\alpha_1\alpha_4 + \alpha_2\alpha_3)}{2}$$

The choice of one of the two γ^o is then arbitrary. Among the infinity of solutions the most symmetrical one is

$$\gamma_1^o = \mu_o \frac{\alpha_1\alpha_3 + \alpha_2\alpha_4}{2} \qquad \gamma_2^o = \mu_o \frac{\alpha_1\alpha_4 + \alpha_2\alpha_3}{2}$$

We get the results

$$a_2 = - a_5\gamma_2^o - a_4 (\gamma_1^o + \gamma'_1 \frac{T}{\mu_o})a_1 + \gamma_1^o$$

$$a_3 = - a_4\gamma_2^o - a_5 (\gamma_1^o + \gamma'_1 \frac{T}{\mu_o})a_1 + (\gamma_2^o + \gamma'_2 \frac{T}{\mu_o})a_1$$

APPENDIX B

Calculation of the a' and b' coefficients introduced in 2.4

A. Long wave, general case

Our three input parameters are T optical thickness

$w = 1-k$ single scattering albedo

and A1 integral factor of the scattering phase function

Let us symbolise by D the differential operator $d(\ )/d(kT)$ with $(1-k)T$ constant. (kT is the absorption optical thickness which will be increased and $(1-k)T$ the scattering optical thickness which will not be affected in the process).

We have $DT = 1$ $DW = -W/T$ and $DA_1 = 0$

The expressions for the computation of b_1 and b_2 are:

$$\alpha_1 = 2.(1 - w.A_1) \quad \alpha_2 = 2.w.(1 - A_1) \quad \varepsilon = \sqrt{\alpha_1^2 - \alpha_2^2}$$

$$\beta_1 = (\alpha_1 - \varepsilon)/\alpha_2 \qquad \tau_1 = e^{-\varepsilon T}$$

$$b_1 = \tau_1.(1 - \beta_1^2)/(1 - \beta_1^2.\tau_1^2) \quad b_2 = \tau_1.(1 - \tau_1^2)/(1 - \beta_1^2.\tau_1^2)$$

A differentiation step by step leads us to

$$b'_1 = Db_1 = (4\beta_1\tau_1 \frac{b_2}{T} - 2(1 + \beta_1^2\tau_1^2)\alpha_1 b_1)/(\varepsilon(1 - \beta_1^2\tau_1^2))$$

$$b'_2 = Db_2 = (4\beta_1\tau_1\alpha_1 b_1 - 2(1 + \beta_1^2\tau_1^2) \frac{b_2}{T})/(\varepsilon(1 - \beta_1^2\tau_1^2))$$

For the computation of b_5 and b_6 we have

$$\lambda = 1/((\alpha_1 + \alpha_2).T)$$

$$b_5 = (1 - b_1 + b_2).\lambda - b_1 \quad b_6 = 1 - b_2 - (1 - b_1 + b_2)\lambda$$

The result of the differentiation is here

$$b'_5 = Db_5 = (b'_2 - b'_1).\lambda - 2.\lambda^2.(1 - b_1 + b_2) - b'_1$$

$$b'_6 = Db_6 = (b'_1 - b'_2).\lambda + 2.\lambda^2.(1 - b_1 + b_2) - b'_2$$

B. Long wave, case without absorption

Although we know the formal expressions of b_1 and b_2 we can no longer take their derivative as in the previous case, since the introduction of a kT is in contradiction with the condition k = o. We must therefore compute a limited expansion of b_1 and b_2 in the neighbourhood of the values obtained for k = o.

We have, for the input parameters, with kT = x

$T = To + x \qquad w = 1 - x/To + x^2/To^2 \ldots \qquad A1$ constant

We get with $u = \alpha T$

$$b_1 = \frac{1}{1+u}\left(1 - x\,\frac{8 + 8u + (8/3)u^2}{4 + 4u}\right)$$

$$b_2 = \frac{u}{1+u}\left(1 - x\,\frac{8 + (16/3)u}{4 + 4u}\right)$$

Thus:

$$b'_1 = -(1 + b_1^2 - b_2^2/3) \qquad b'_2 = -(1 - b_1^2 + b_2^2/3)$$

The results for b'_5 and b'_6 are the same as in part A. with $\lambda = 1/(2u)$

Thus:

$$b'_5 = b_1 + 2b_2/3 \qquad b'_6 = b_1 + 4b_2/3$$

C. Short wave, general case

We have two supplementary input parameters. μo cosine of the solar zenith angle and its dependent integral factor of the phase function A3(μo).

Both of them are unchanged in the differentiation process : $D\mu_o = 0 \quad DA_3 = 0$

The results for a'_4 and a'_5 are the same as those for b'_1 and b'_2

As $a_1 = e^{-T/\mu_o}$ $\qquad$ $\boxed{a'_1 = -a_1/\mu_o}$

The expressions for the computation of a_2 and a_3 are

$$\alpha_3 = wA_3 \qquad \alpha_4 = w(1 - A_3)$$

$$\gamma_1 = -\frac{(\alpha_1\alpha_3 + \alpha_2\alpha_4)\mu_o - \alpha_3}{1 - \varepsilon^2\mu_o^2} \qquad \gamma_2 = -\frac{(\alpha_1\alpha_4 + \alpha_2\alpha_3)\mu_o + \alpha_4}{1 - \varepsilon^2\mu_o^2}$$

$$a_2 = -a_5\gamma_2 - a_4\gamma_1 a_1 - \gamma_1 \qquad a_3 = -a_4\gamma_2 - a_5\gamma_1 a_1 - \gamma_2 a_1$$

Thus to compute a'_2 and a'_3 we only need to know $D\gamma_1$ and $D\gamma_2$.

The differentiation step by step leads to

$$D\gamma_1 = \gamma_1(2\mu_o^2(2\alpha_1-\varepsilon^2)/(1-\varepsilon^2\mu_o^2) - 2)/T - \alpha_3(2\mu_o-1)/(T(1-\varepsilon^2\mu_o^2))$$

$$D\gamma_2 = \gamma_2(2\mu_o^2(2\alpha_1-\varepsilon^2)/(1-\varepsilon^2\mu_o^2) - 2)/T - \alpha_4(2\mu_o+1)/(T(1-\varepsilon^2\mu_o^2))$$

and finally

$$a'_2 = -a'_5\gamma_2 - a_5 D\gamma_2 - a'_4\gamma_1 a_1 - a_4(D\gamma_1 a_1 + \gamma_1 a'_1) + D\gamma_1$$

$$a'_3 = -a'_4\gamma_2 - a_4 D\gamma_2 - a'_5\gamma_1 a_1 - a_5(D\gamma_1 a_1 + \gamma_1 a'_1) + D\gamma_2 a_1 + \gamma_2 a'_1$$

D. Short wave, resonance case

The results obtained in C. for a'_1 a'_4 and a'_5 remains valid.

But for a'_2 and a'_3, as in B., we can no longer derive the final expressions of a_2 and a_3. But in this case the calculation of the derivative is simplified since we can compute a limited expansion by varying an independent parameter, namely μ_o.

We take $\mu_o = (1 + y)/\varepsilon$ and the results for a'_2 and a'_3 are of the type $(0 + my^2)/(0 + ny^2) = m/n$

The result is quite complicated :

With the $\gamma_1^o \gamma_2^o \gamma'_1 \gamma'_2$ from Appendix A

and

$$\delta_1^o = -\frac{1}{T}.((4\gamma_1^o + 2\gamma'_1).\alpha_1\mu_o^2 - \alpha_3.(6\mu_o - 1)/4)$$

$$\delta_2^o = -\frac{1}{T}.((4\gamma_2^o + 2\gamma'_2).\alpha_1\mu_o^2 - \alpha_4.(6\mu_o + 1)/4)$$

$$\delta'_1 = -\frac{1}{T}.((2\gamma_1^o + 4\gamma'_1).\alpha_1\mu_o^2 - \gamma_1^o - \alpha_3.(2\mu_o - 1)/2)$$

$$\delta'_2 = -\frac{1}{T}.((2\gamma_2^o + 4\gamma'_2).\alpha_1\mu_o^2 - \gamma_2^o - \alpha_4.(2\mu_o + 1)/2)$$

$$\delta''_1 = -\frac{1}{T}.\gamma'_1.(2\alpha_1\mu_o^2 - 1)$$

$$\delta''_2 = -\frac{1}{T}.\gamma'_2\ (2\alpha_1\mu_o^2 - 1)$$

we have

$$a'_2 = -a_5\delta_2^o - \frac{a'_5}{2}(\gamma'_2 + 2\gamma_2^o) - a_4\left[a_1(\delta_1^o + (\delta'_1 - \delta''_1)\frac{T}{\mu_o} + \frac{\delta''_1}{2}\frac{T^2}{\mu_o^2}) + \frac{a'_1}{2}(2\gamma_1^o - \gamma'_1 + 2\gamma'_1\frac{T}{\mu_o})\right] - \frac{a'_4 a_1}{2}(\gamma'_1 + 2\gamma_1^o + 2\gamma'_1\frac{T}{\mu_o}) + \delta_1^o$$

$$a'_3 = -a_4\delta_2^o - \frac{a'_4}{2}(\gamma'_2 + 2\gamma_2^o) - a_5\left[a_1(\delta_1^o + (\delta'_1 - \delta''_1)\frac{T}{\mu_o} + \frac{\delta''_1}{2}\frac{T^2}{\mu_o^2}) + \frac{a'_1}{2}(2\gamma_1^o - \gamma'_1 + 2\gamma'_1\frac{T}{\mu_o})\right] - \frac{a'_5 a_1}{2}(\gamma'_1 + 2\gamma_1^o + 2\gamma'_1\frac{T}{\mu_o})$$
$$+ a_1(\delta_2^o + (\delta'_2 - \delta''_2)\frac{T}{\mu_o} + \frac{\delta''_2}{2}\frac{T^2}{\mu_o^2}) + \frac{a'_1}{2}(2\gamma_2^o - \gamma'_2 + 2\gamma'_2\frac{T}{\mu_o})$$

APPENDIX C

Combination of partially covered cloud layers

We are treating here the simplest case of two adjacent cloudy layers A(above) and B(below) with partial cloud coverages C_A and C_B (here $C_A<C_B$) and we are looking for the a and b coefficients of the layer A knowing the ones for cloudy (1) and clear (0) conditions in both layers. All of the following can easily be extended to any layer in any cloud configuration.

The geometry of our "cloud" is (with the coefficients in the corresponding spaces)

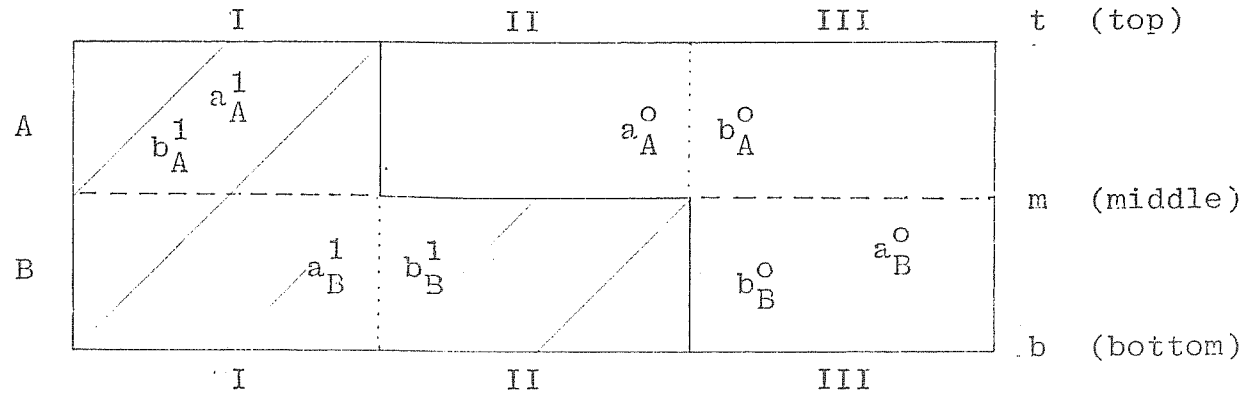

A) Short wave fluxes With a* and b* representing a^1 and b^1 or a^o and b^o depending on case k = I, II or III (different vertical repartitions of cloudy and non cloudy conditions) we can write our linear equation system for the fluxes (see equation (9))

$$\begin{bmatrix} 1 & & & & & & & & \\ & 1 & & & & & & 0 & \\ -a_A^{*6} & -a_A^{*2} & 1 & & -a_A^{*4} & & & & \\ -a_A^{*7} & -a_A^{*3} & & 1 & -a_A^{*5} & & & & \\ & -a_A^{*1} & & & 1 & & & & \\ & & -a_B^{*6} & -a_B^{*2} & 1 & & -a_B^{*4} & & \\ & & -a_B^{*7} & -a_B^{*3} & & 1 & -a_B^{*5} & & \\ & & & -a_B^{*1} & & & 1 & & \\ & 0 & & & & & & 1 & \end{bmatrix} \begin{bmatrix} F_{2t} \\ S_t \\ F_{1t} \\ F_{2m} \\ S_m \\ F_{1m} \\ F_{2b} \\ S_b \\ F_{1b} \end{bmatrix}^k = \begin{bmatrix} F_{2t} \\ S_t \\ 0 \\ 0 \\ 0 \\ 0 \\ 0 \\ 0 \\ F_{1b} \end{bmatrix}$$

We can solve it in each case to get for the layer A matrix equations of the type

$$\begin{bmatrix} S_t \\ F_{1m} \\ F_{2t} \end{bmatrix}^k = \begin{bmatrix} C \end{bmatrix}^k \cdot \begin{bmatrix} S_t \\ F_{1b} \\ F_{2t} \end{bmatrix} \quad \text{and} \quad \begin{bmatrix} S_m \\ F_{1t} \\ F_{2m} \end{bmatrix}^k = \begin{bmatrix} d \end{bmatrix}^k \cdot \begin{bmatrix} S_t \\ F_{1b} \\ F_{2t} \end{bmatrix}$$

for the incoming and outgoing fluxes.

Thus with linear combination and elimination of the fluxes S_t F_{1b} and F_{2t} we obtain the matrix solution from equation (9)

$$\left[a_A\right] = \left[C_A\left[d\right]^I + (C_B - C_A)\left[d\right]^{II} + (1 - C_B)\left[d\right]^{III}\right] \cdot \left[C_A\left[c\right]^I + (C_B - C_A)\left[c\right]^{II} + (1 - C_B)\left[c\right]^{III}\right]^{-1}$$

B) Long wave fluxes The computation of coefficients $b_{1\ldots4}$ is the same as the one described above for the $a_{1\ldots\ldots7}$

For the other ones we change the formalism of equation (10) and replace the product $\begin{bmatrix} b_5 & b_7 \\ b_6 & b_8 \end{bmatrix} \cdot \begin{bmatrix} \pi B_b \\ \pi B_t \end{bmatrix}$ by the resulting vector $\begin{bmatrix} e_1 \\ e_2 \end{bmatrix}$

Then we first make a computation similar to the one already done for the determination of the $b_{1..4}$ coefficients, without incoming fluxes but with local emission (see equation (10)).

$$\begin{bmatrix} 1 & & & & 0 & \\ -b_A^*3 & 1 & & -b_A^*1 & & \\ -b_A^*4 & & 1 & -b_A^*2 & & \\ & & -b_B^*3 & 1 & & -b_B^*1 \\ & & -b_B^*4 & & 1 & -b_B^*2 \\ 0 & & & & & 1 \end{bmatrix} \cdot \begin{bmatrix} F_{2t} \\ F_{1t} \\ F_{2m} \\ F_{1m} \\ F_{2b} \\ F_{1b} \end{bmatrix}^k = \begin{bmatrix} 0 \\ e_A^*1 \\ e_A^*2 \\ e_B^*1 \\ e_B^*2 \\ 0 \end{bmatrix}$$

Then we again make a linear combination and eliminate the unwanted fluxes from equation (10).

$$\begin{bmatrix} e_A{}^1 \\ \\ e_A{}^2 \end{bmatrix} = \left[C_A \begin{bmatrix} F_{1t} \\ \\ F_{2m} \end{bmatrix}^{I} + (C_B - C_A) \begin{bmatrix} F_{1t} \\ \\ F_{2m} \end{bmatrix}^{II} + (1 - C_B) \begin{bmatrix} F_{1t} \\ \\ F_{2m} \end{bmatrix}^{III} \right]$$

$$- \begin{bmatrix} b_A{}^1 & b_A{}^3 \\ \\ b_A{}^2 & b_A{}^4 \end{bmatrix} \cdot \left[C_A \begin{bmatrix} F_{1m} \\ \\ F_{2t} \end{bmatrix}^{I} + (C_B - C_A) \begin{bmatrix} F_{1m} \\ \\ F_{2t} \end{bmatrix}^{II} + (1 - C_B) \begin{bmatrix} F_{1m} \\ \\ F_{2t} \end{bmatrix}^{III} \right]$$

APPENDIX D

Generation of random atmospheres

There are 15 levels equally spaced between 0 and 1 in the coordinate system q with $\sigma = p/p_s = \sin^2(q\pi/2)$

We start from the ground with $p_s = 1013.25$ mb. and $T_s = 288.15^{\circ}K$ and going upwards for each layer we generate randomly the temperature lapse rate dT/dz and two relative humidities U_1 and U_2 under the following conditions:

$\frac{dT}{dz} = \frac{g}{c_p}(f_1 - 1)$ f_1 having a log-normal distribution with mean value $1-\sigma$ and variance σ/α

$U_{1,2} = f_2$ f_2 having a log-normal distribution with mean value σ and variance $(1-\sigma).\alpha$

U_1 and U_2 represent a maximum and a minimum relative humidity and we have assumed a rectangular distribution between these values for the relative humidities in the layer.

This gives us the cloud cover and the mixing ratios of water vapour and liquid water (with the temperature linearly interpolated with respect to pressure in the middle, for the coordinate q, of the layer).

The arbitrary parameter α is adjusted so that the mean cloud cover is equal to 0.5. For the computation of the parameter we suppose that adjacent cloudy layers have a maximum overlapping of their cloudy parts and that distinct "clouds" are randomly distributed with respect to each other. Thus we have to take $\alpha = 0.76$.

3. A comparative experiment for two radiation schemes

3.1 The experiment

Our basic model was a combination of the ECMWF adiabatic grid point model and of the GFDL physical package with the saturation criterion set to 100%. The very coarse resolution of 7.5^{o} in latitude and 11.25^{o} in longitude was chosen to allow long term integrations with acceptable computer time consumption. From real data for the 1st March 1965 we made a 50 day integration (which will now be referred to as GFD) and then replaced the GFDL radiation scheme by ours, making the humidity interactive. The water vapour mixing ratio being given, the only problem was to define cloudiness and liquid water content. Totally arbitrarily we took $C = \left[\max(o, \frac{U-\sigma}{1-\sigma})\right]^2$ (C cloudiness, U relative humidity, σ vertical coordinate) and $q\ell = o$ ($q\ell$ liquid water mixing ratio before adsorption of water vapour by aerosols). Since there is no precipitation associated with relative humidities between σ and 1 we must have too much cloudiness in the upper atmospheric layers but with very few aerosols there the liquid water optical depth will remain low. Surprisingly these arbitrary assumptions proved sufficient for our purpose, although we can say that our scheme had the disadvantage to interact with other parameterisations with which it had not been tuned. We made three integrations from the same initial data set with three different boundary conditions for T_{∞}. The first case was with the same condition as in the GFDL scheme: $T_{\infty} = 200^{o}K$ everywhere and constant in time. The run (referred to as RT2) stopped at day 26, the reason being an instability of the horizontal diffusion scheme for modes probably initiated by the advection of moisture violating the CFL condition (14 m/s in this case), as described in our first chapter. A second run (referred to as RTE) was done with T_{∞} extrapolated linearly with respect to pressure from the two last layers and it was down at day 44. Eventually a run (referred to as RTC) in which T_{∞} was kept constant in time and equal to its extrapolated value in the initial state succeeded in reaching 50 days. However, in the last two runs there were very strange features near the north pole where a very strong wave number one stratospheric pattern was observed in the initial state and produced either forced or oscillating waves through the boundary condition, and therefore the problem remains unsolved.

3.2 Some results

Among the great quantity of information we obtained from these four runs we will present here three kinds of results which we believe to be the more interesting ones: - first, a study of the divergence between GFD and RT2 on 25 days. Figures 1 to 4 give comparisons of the 500 mb and 1000 mb heights north of $20^{o}N$ at 10 and 20 days for both runs. At 10 days there is hardly an important difference in the 500 mb

patterns and at 1000 mb the most important phenomena is an increase in the intensity of pressure centres for RT2 beside quite distinct patterns over Central Asia. At 20 days, however, the 500 mb flow is totally different, the GFD run going towards zonalisation and the RT2 one having created a new circulation type. At the surface of course the same is true, although the situations over Europe and the East coast of Asia are very similar and may have resulted from the same development in both runs. The conclusion of these comparisons should be that interactive radiation is only important in a ten day forecast by creating some more available potential energy in middle waves but, since the phenomena studied here is more continuous as it appears and is likely to be bound to the resolution, it may be that with a fine mesh the kind of discrepancies observed here at 20 days appear earlier and are important for a 10 day forecast. This argument is reinforced by the study of the RMS differences and correlation of heights on Figures 5 to 8 where variations with time, height and latitude are plotted. In contradiction to what could be expected from the charts there is no sudden change in the averaged "speed of divergence" between both integrations, but such a phenomena can be observed locally at high latitudes. The minimum of differences is observed at 50-60°N and 700-800 mb for the zonal flow as well as for long and middle waves. This is also the domain of the highest correlations in terms of latitude, but the vertical repartition is very different, the best agreement appearing in the upper atmosphere and strong differences at the ground, especially for the zonal flow and very early. The surprising thing in the latter feature is that it is not obvious in the 1000 mb charts.

- second, a comparison of the energetics for GFD and RTC on 50 days. Figures 9 to 11 show the evolution of CK (convection of eddy to zonal kinetic energy), CA (the reverse for available potential energy), KE (kinetic energy) and AE (available potential energy). One can see that there is a very strong shock for RTC around day 35 (probably the same kind of thing that causes the breakdown of RT2 and RTE), but that it recovers from it. As noticed in the charts, the interactive scheme creates more available potential energy in the waves and also more kinetic energy in the long waves (all encouraging features), but this is at the expense of the intensity of the zonal flow, the conversion CK being missed more in RTC than in GFD. The question is whether both positive and negative phenomena have something to do with our cloud parameterisation or not.

- third, a picture of radiation properties for the different runs. Downward net fluxes at the surface and vertical integrated divergences are plotted against latitude in Figures 12 and 13 for days 25 and 50. The averaged vertical profiles of cooling rates interpolated in tropospheric standard pressure levels are shown on Figure 14 for the same days. The first obvious thing is that the boundary condition at T_∞ is surprisingly more important for the dynamic as for the radiation itself as

the curves for RT2, RTE and RTC are very similar in the three figures. But the most important thing about these results, and probably about the whole experiment, is that they give very similar properties for our radiation scheme as the ones we noticed in the last chapter (if, of course, we consider the GFDL scheme as representative of "the truth", which we can do given its humidity climatological features). We have very good surface fluxes both in average and in zonal repartition and again too high cooling rates, but with a similar vertical repartition except for the boundary layer. This discrepancy is mainly due to the way in which the GFDL model computes long wave fluxes on continents: first the downward fluxes are obtained, then the one at the surface is used to diagnose the surface temperature used in the computation of upward fluxes. This artificially suppresses the cooling of the lowest layer, probably because it would create trouble with the stability independent boundary layer scheme. The only new "real" difference is in the zonal variation of the integrated cooling rates, maximum at the poles for GFD and in the tropics for RT2, RTE and RTC. A comparison with direct climatological computations (see for example Figures 1-10 of Paltridge and Platt ,1976) show that our profile is more realistic, but it is probably the cause of the decrease in the zonal kinetic energy. This gives a possible answer to the question above: there is a lack in the release of latent heat in the tropics in the GFDL convection scheme which is compensated by a too low radiative cooling. However, the similarity between the results of our scheme in these integrations and in the slab test computations, means either a very lucky choice of the cloud parameterisation or a quick adaptation of the radiation input to some general constraints. If the latter is true, and it seems to be so since there are strong differences at the initial state, this would be a very strong argument for the use of interactive radiation.

In any case, all tests proved the reliability of our scheme, the inadequacy of its transmission functions, the need for further studies about T_∞ and about some stability problems which can hopefully be solved by a better balance between time and space radiation scales.

Figure 1

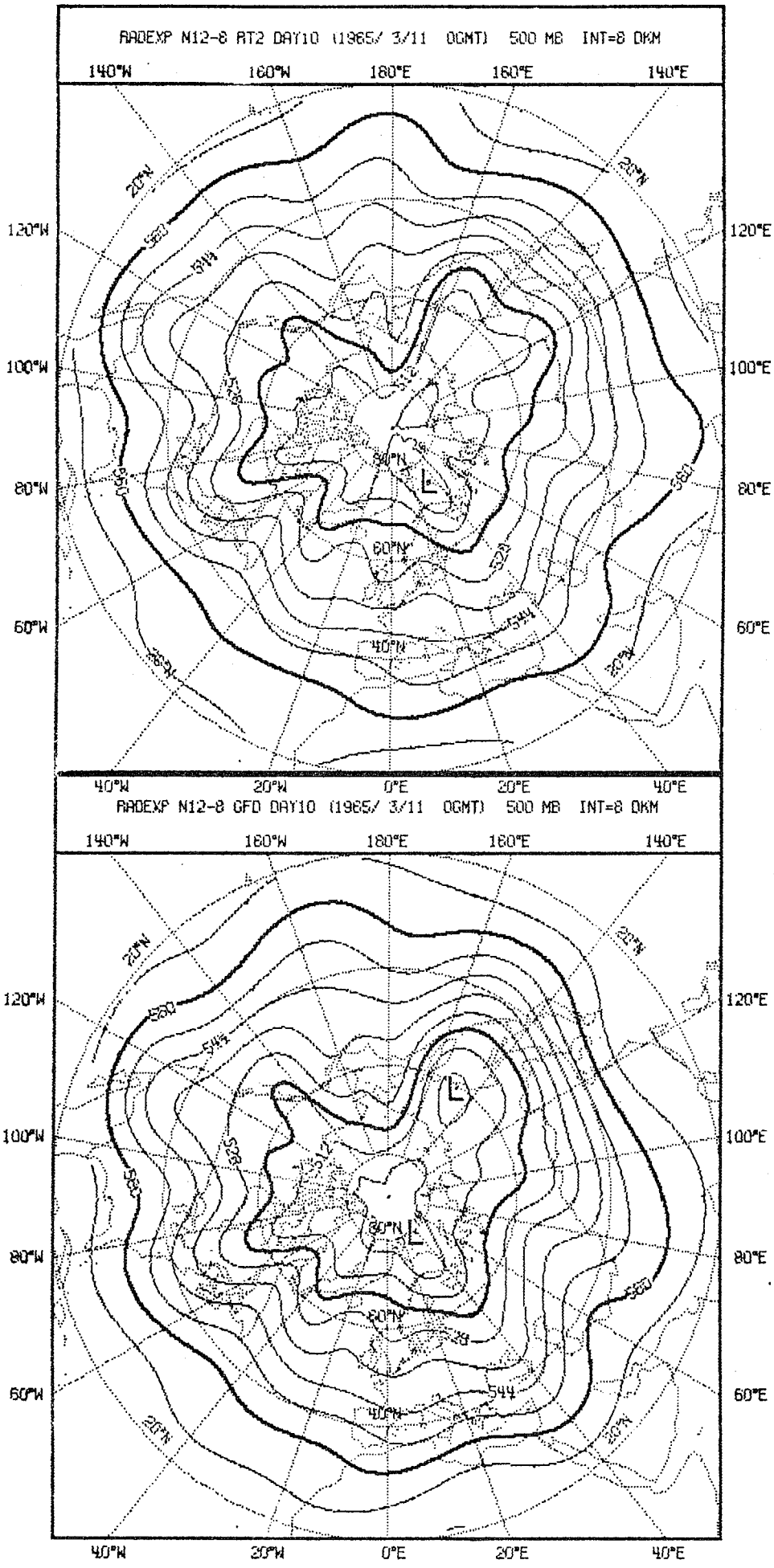
RADEXP N12-8 RT2 DAY10 (1985/ 3/11 0GMT) 500 MB INT=8 DKM
140°W
160°W
180°E
160°E
140°E
120°W
100°W
80°W
60°W
120°E
100°E
80°E
60°E
20°N
40°N
60°N
520
544
568
40°W
20°W
0°E
20°E
40°E
RADEXP N12-8 GFD DAY10 (1985/ 3/11 0GMT) 500 MB INT=8 DKM
140°W
160°W
180°E
160°E
140°E
120°W
100°W
80°W
60°W
120°E
100°E
80°E
60°E
20°N
40°N
60°N
520
544
568
40°W
20°W
0°E
20°E
40°E

Figure 2

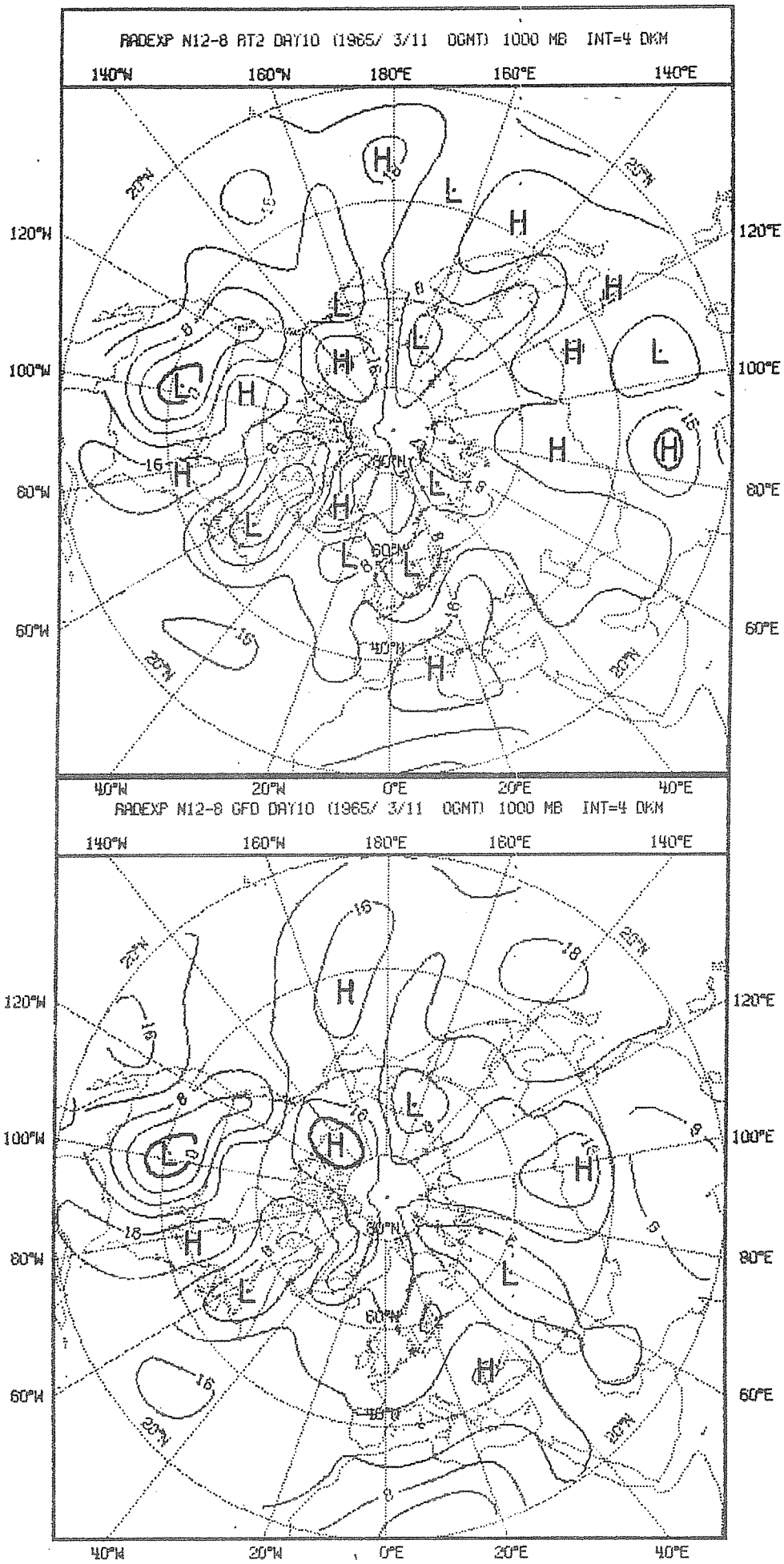
RADEXP N12-8 AT2 DAY10 (1965/ 3/11 0GMT) 1000 MB INT=4 DKM
140°W
160°W
180°E
160°E
140°E
120°W
120°E
100°W
100°E
80°W
80°E
60°W
60°E
40°N
60°N
80°N
40°W
20°W
0°E
20°E
40°E
RADEXP N12-8 GFD DAY10 (1965/ 3/11 0GMT) 1000 MB INT=4 DKM

Figure 3

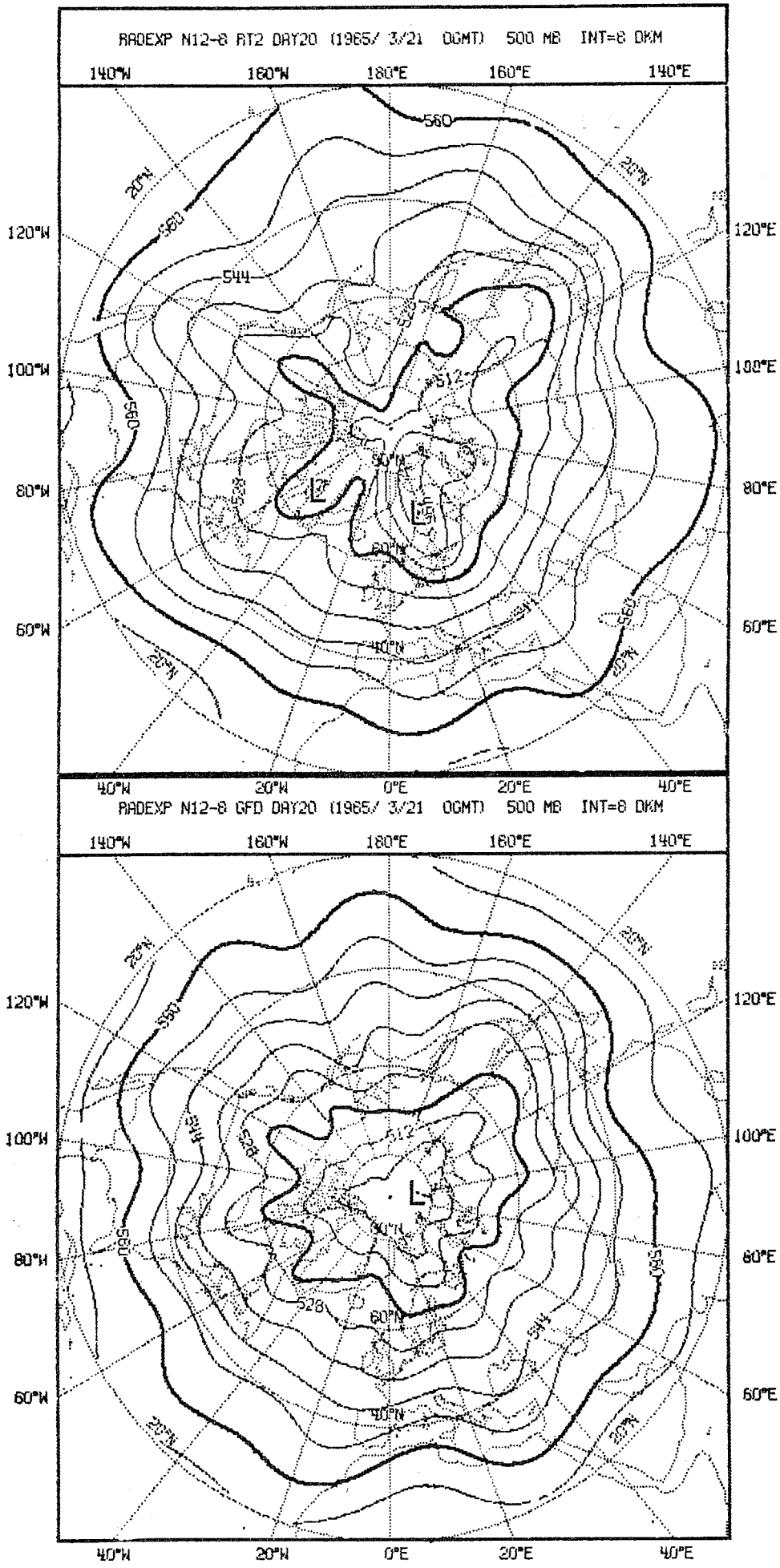
RADEXP N12-8 RT2 DAY20 (1985/ 3/21 0GMT) 500 MB INT=8 DKM
140°W
160°W
180°E
160°E
140°E
120°W
120°E
100°W
100°E
80°W
80°E
60°W
60°E
40°W
20°W
0°E
20°E
40°E
20°N
40°N
60°N
80°N
560
544
528
512
RADEXP N12-8 GFD DAY20 (1985/ 3/21 0GMT) 500 MB INT=8 DKM
140°W
160°W
180°E
160°E
140°E
120°W
120°E
100°W
100°E
80°W
80°E
60°W
60°E
40°W
20°W
0°E
20°E
40°E
20°N
40°N
60°N
80°N
560
544
528
512

Figure 4

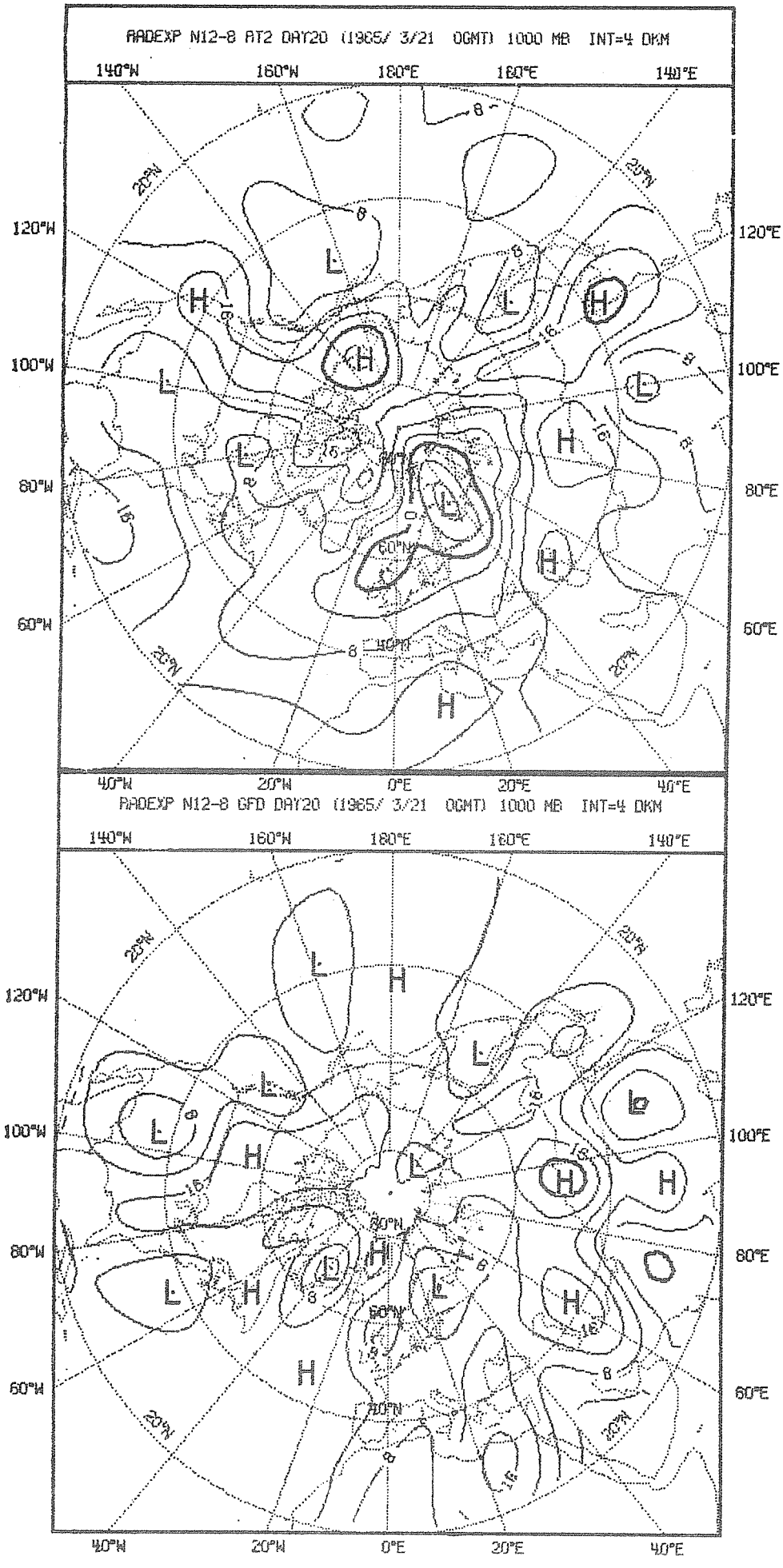
RADEXP N12-8 BT2 DAY20 (1985/ 3/21 0GMT) 1000 MB INT=4 DKM
140°W
160°W
180°E
160°E
140°E
120°W
100°W
80°W
60°W
120°E
100°E
80°E
60°E
20°N
40°W
20°W
0°E
20°E
40°E
RADEXP N12-8 GFD DAY20 (1985/ 3/21 0GMT) 1000 MB INT=4 DKM

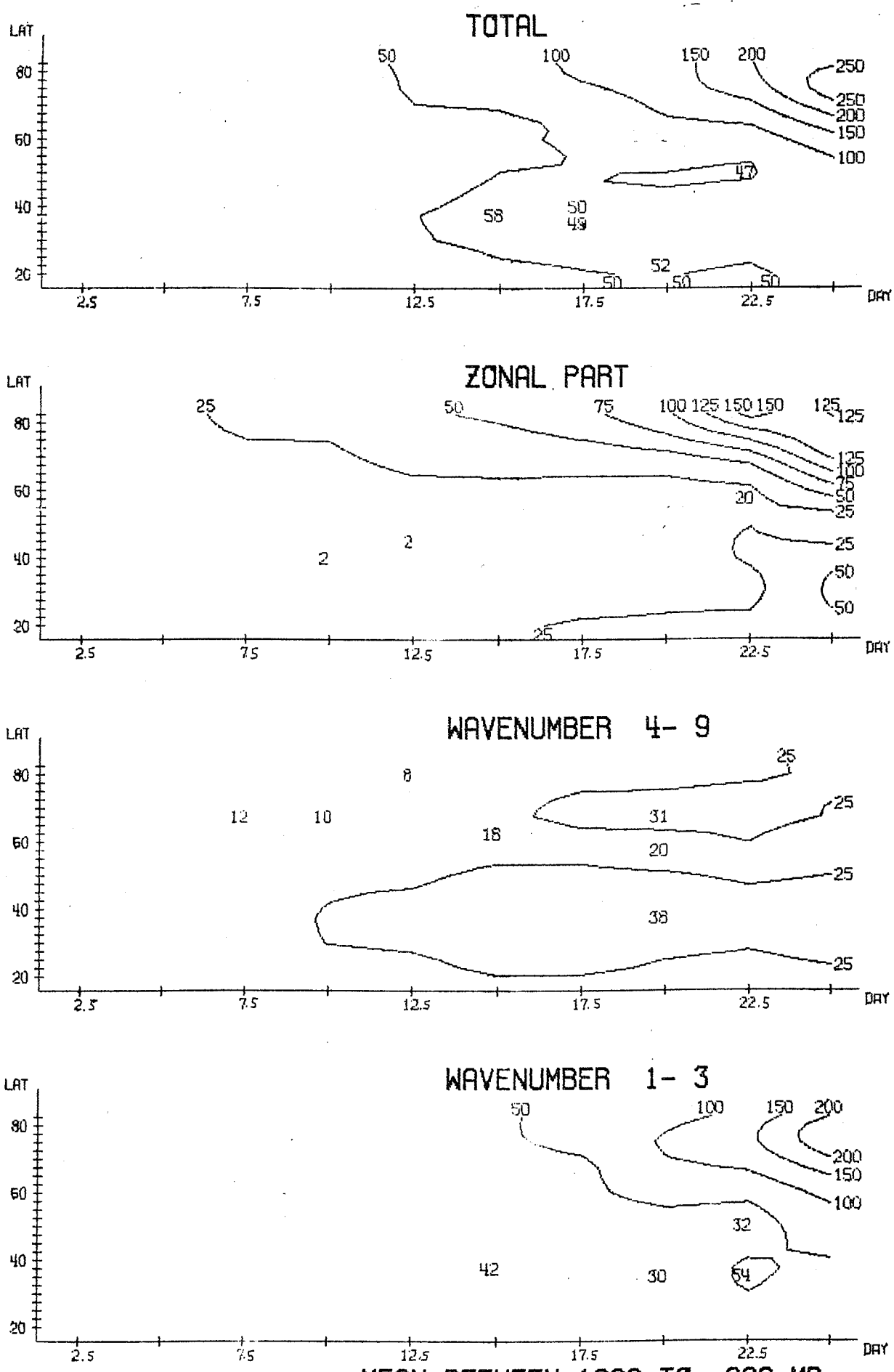

MEAN BETWEEN 1000 TO 200 MB

RMS ERROR OF HEIGHT (M) RT2 VS GFD

Figure 5

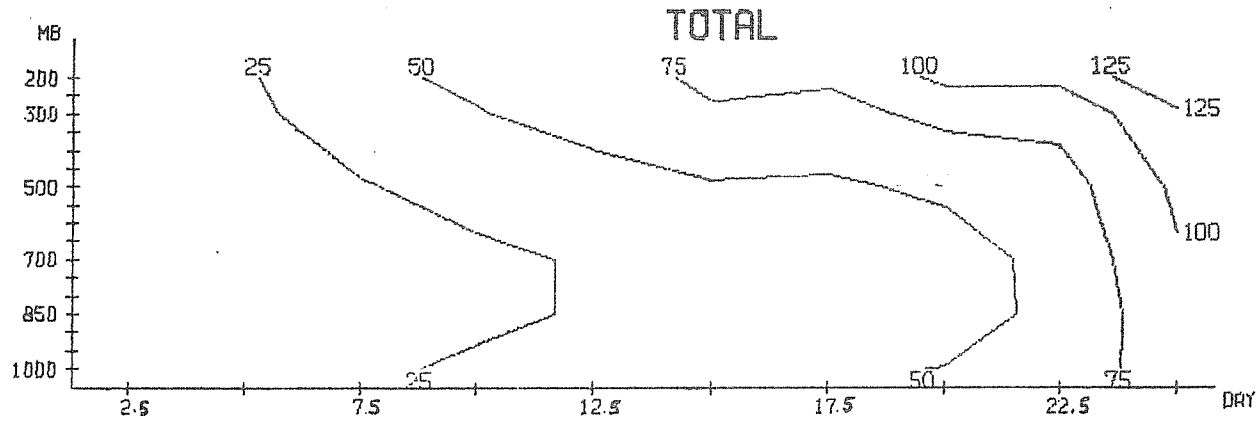

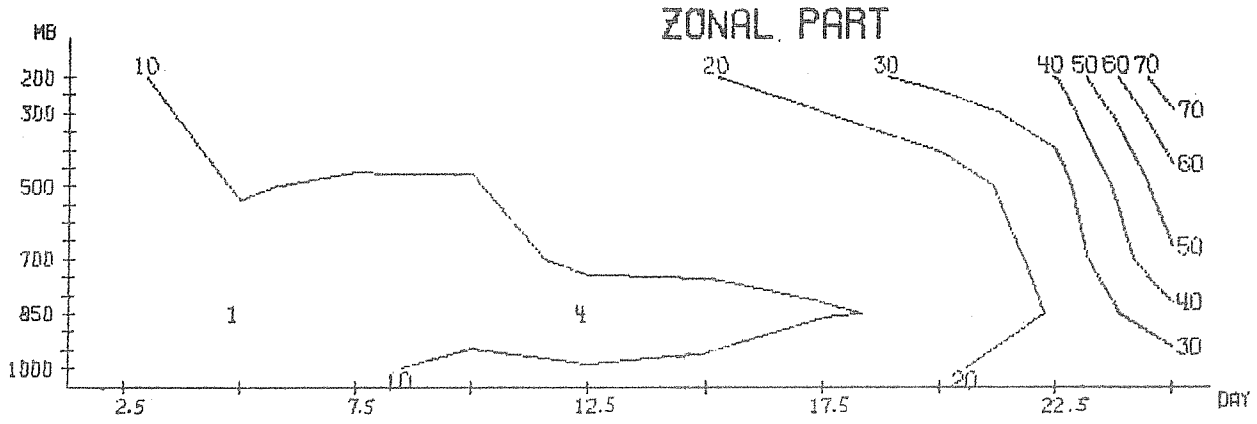

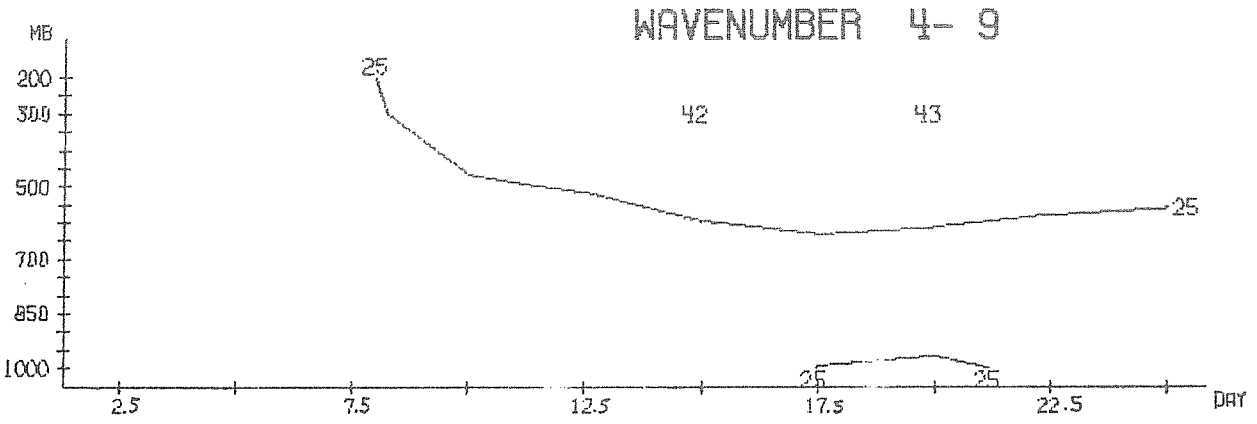

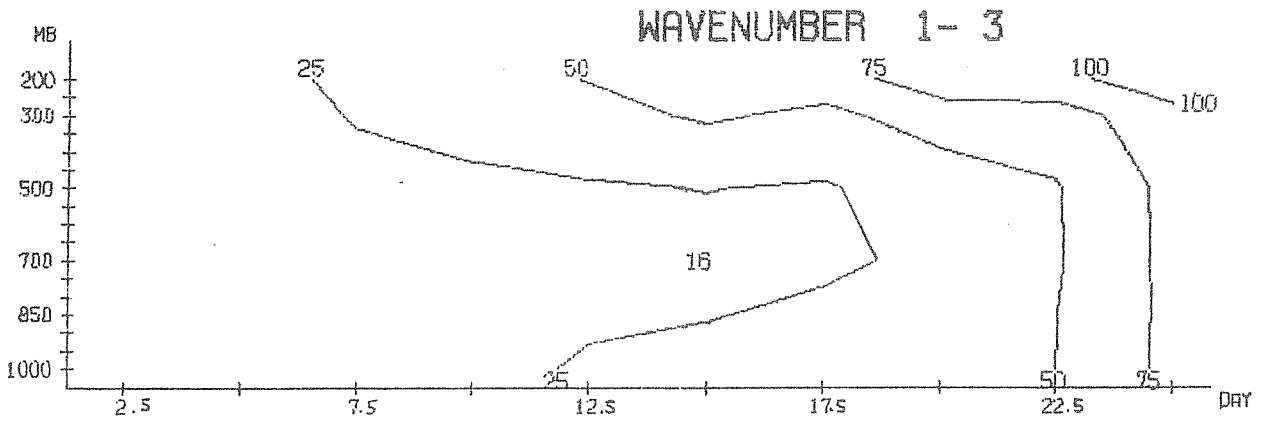

MEAN BETWEEN 30.0 AND 70.0 N

RMS-ERROR OF HEIGHT (M) RT2 VS GFD

Figure 6

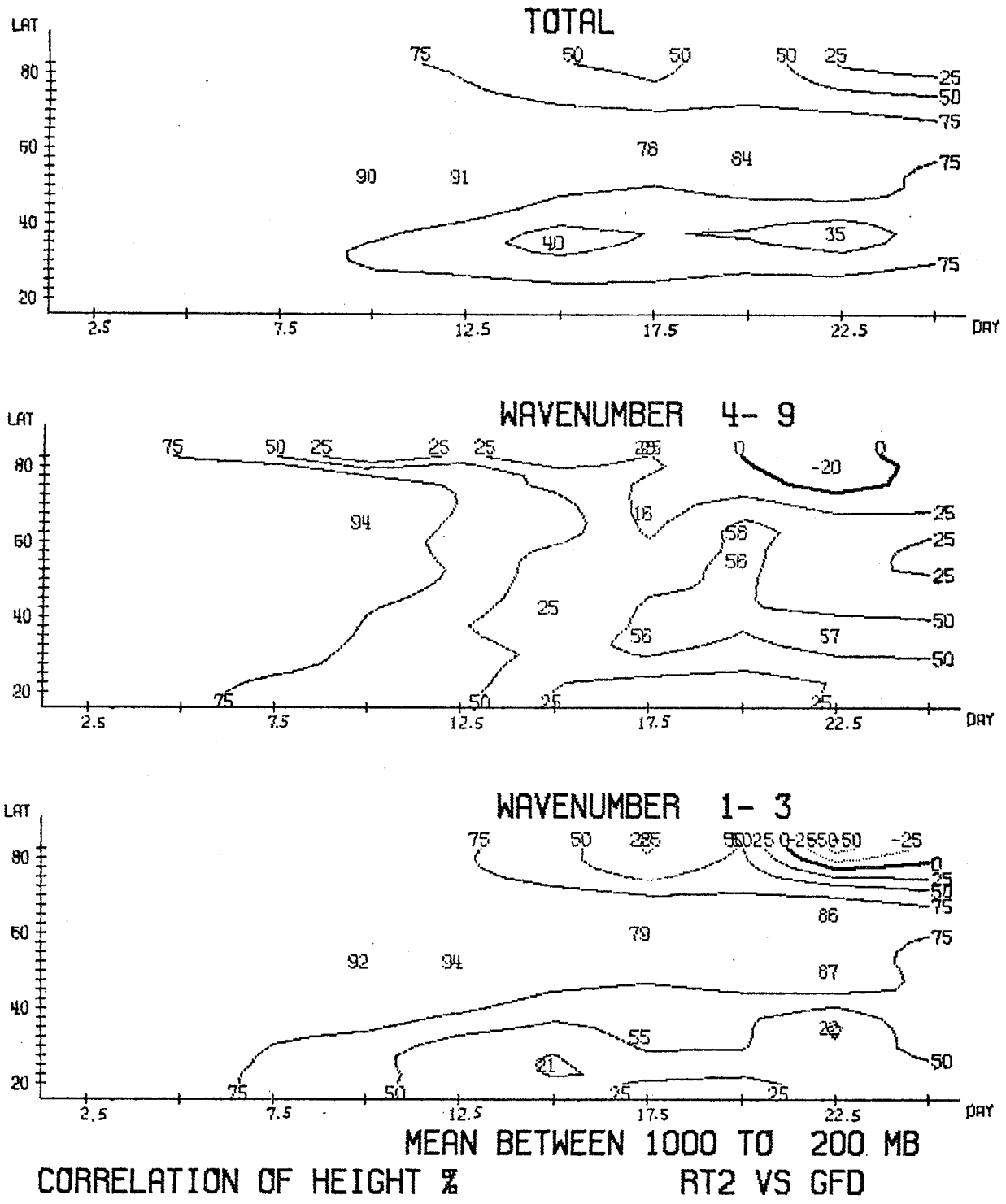

MEAN BETWEEN 1000 TO 200 MB

CORRELATION OF HEIGHT % RT2 VS GFD

Figure 7

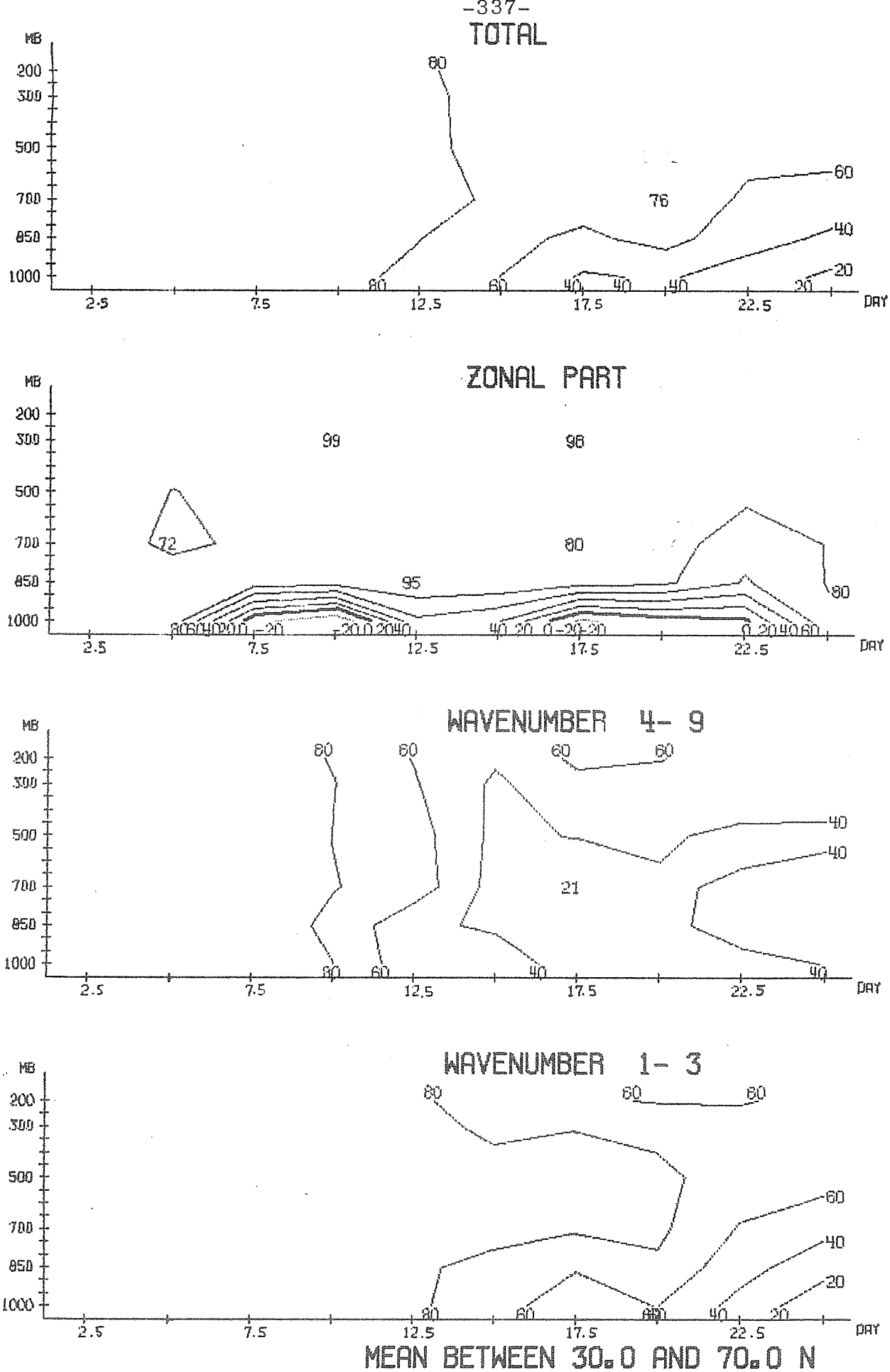

MEAN BETWEEN 30.0 AND 70.0 N

CORRELATION OF HEIGHT % RT2 VS GFD

Figure 8

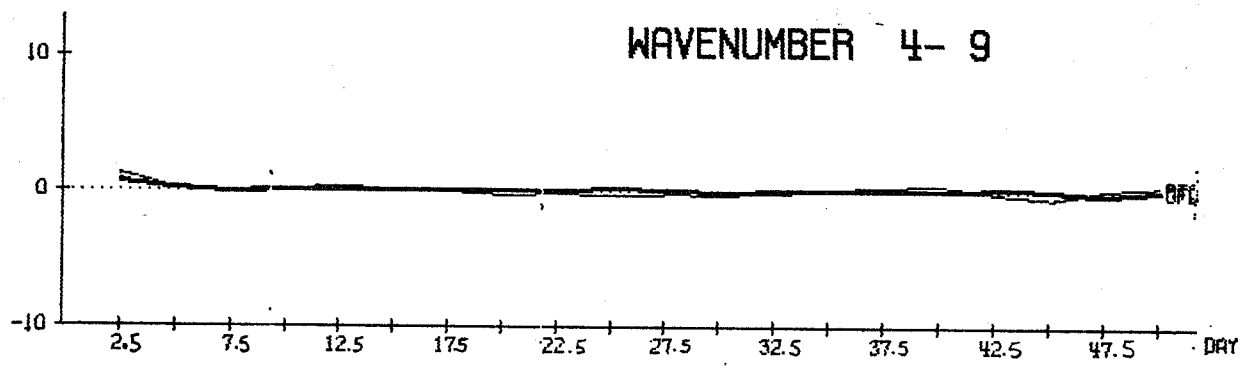

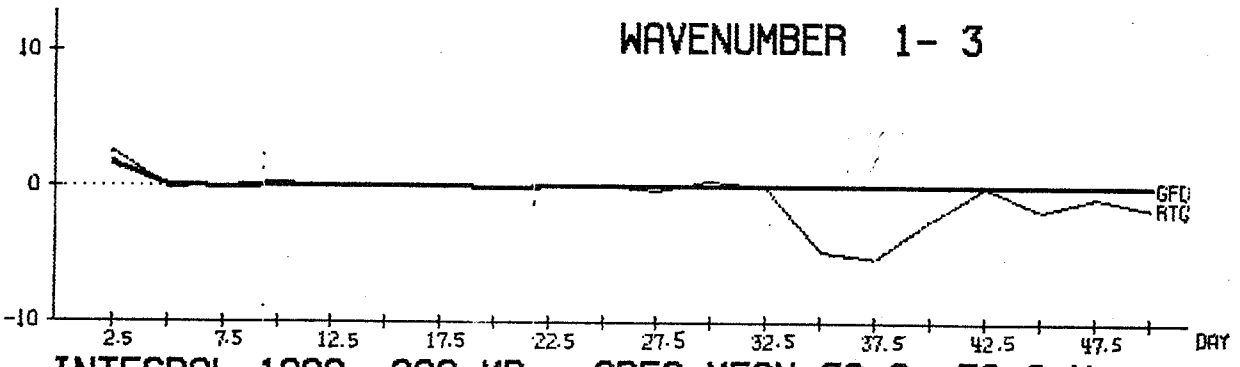

INTEGRAL 1000- 200 MB AREA MEAN 30.0- 70.0 N
CK (1/10 WATT/M2)

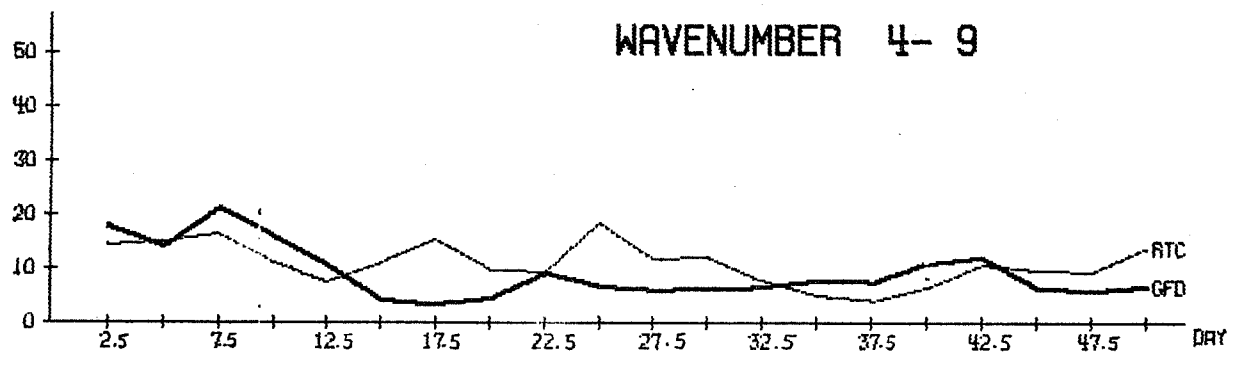

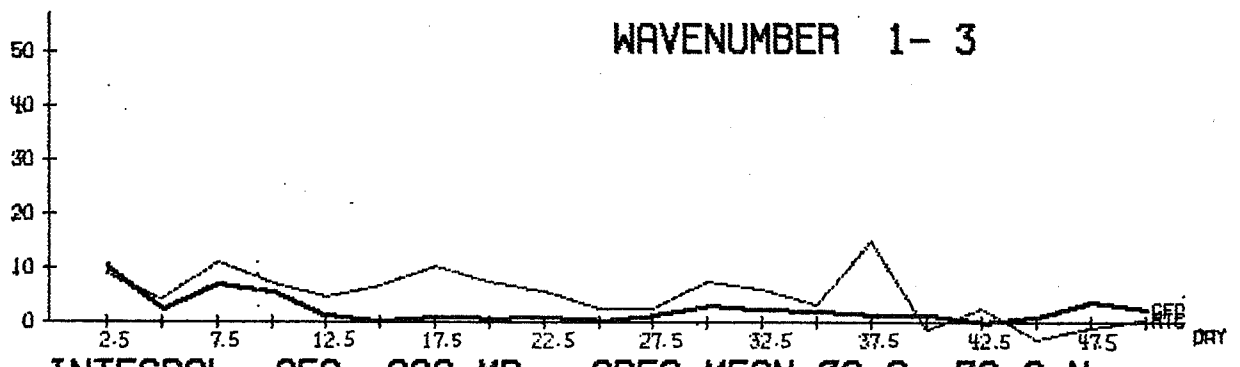

INTEGRAL 850- 200 MB AREA MEAN 30.0- 70.0 N
CA (1/10 WATT/M2)

Figure 9

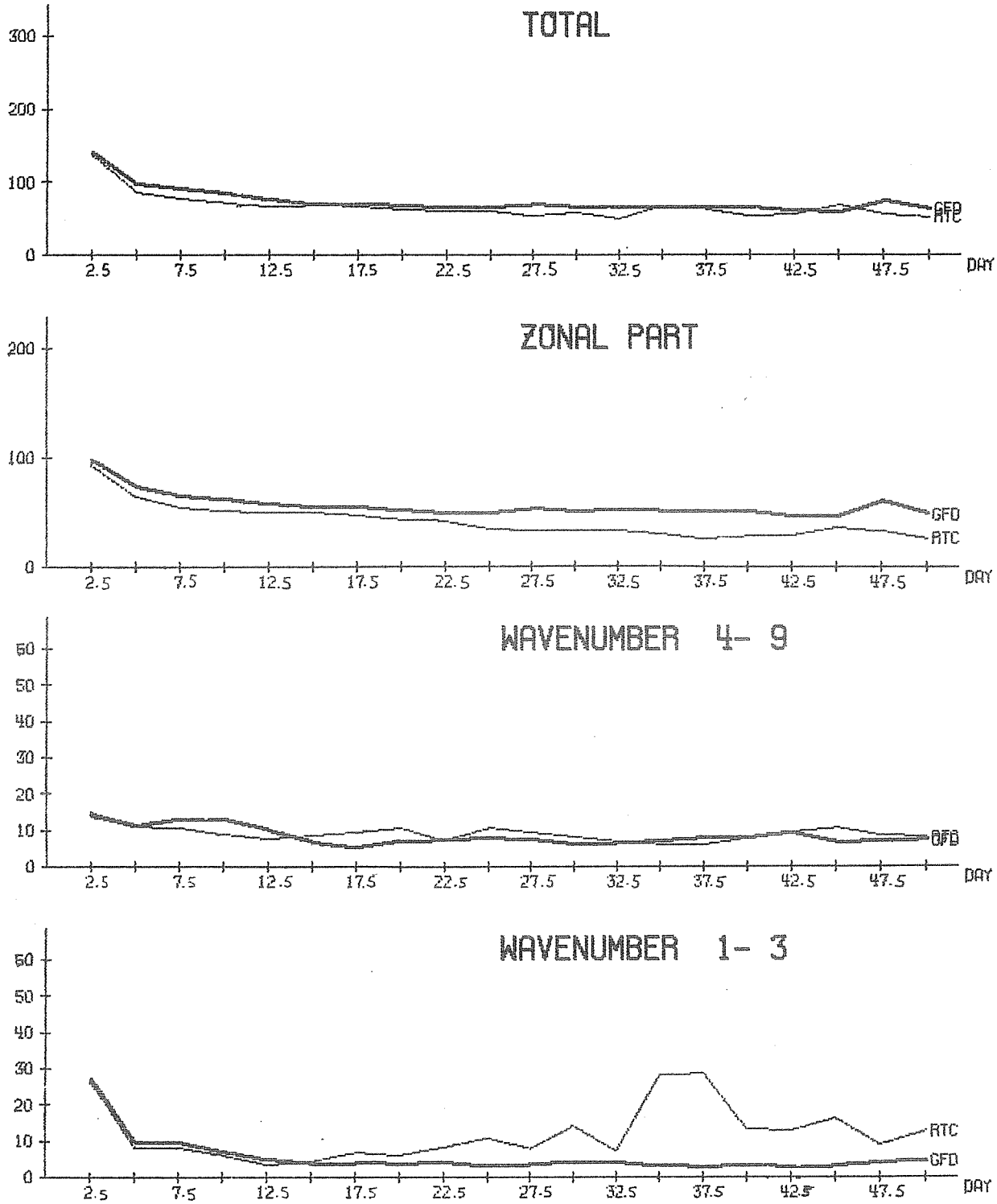
TOTAL
300
200
100
0
2.5
7.5
12.5
17.5
22.5
27.5
32.5
37.5
42.5
47.5
DAY
GFD
RTC
ZONAL PART
200
100
0
GFD
RTC
WAVENUMBER 4- 9
60
50
40
30
20
10
0
GFD
WAVENUMBER 1- 3
RTC
GFD
INTEGRAL 1000- 200 MB AREA MEAN 30.0- 70.0 N
KE (10 KJ/M2)

Figure 10

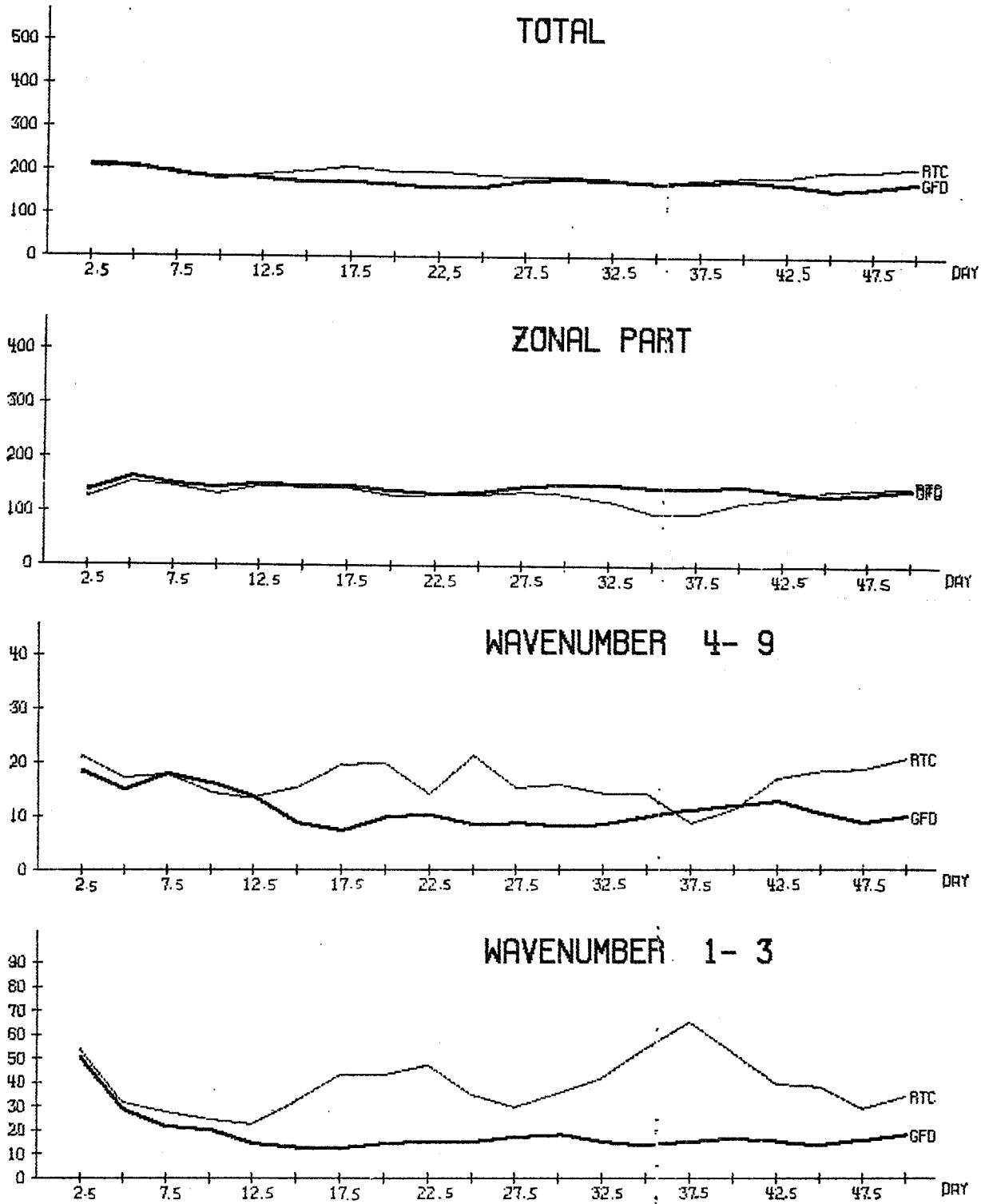

INTEGRAL 850- 200 MB AREA MEAN 30.0- 70.0 N
AE (10 KJ/M2)

Figure 11

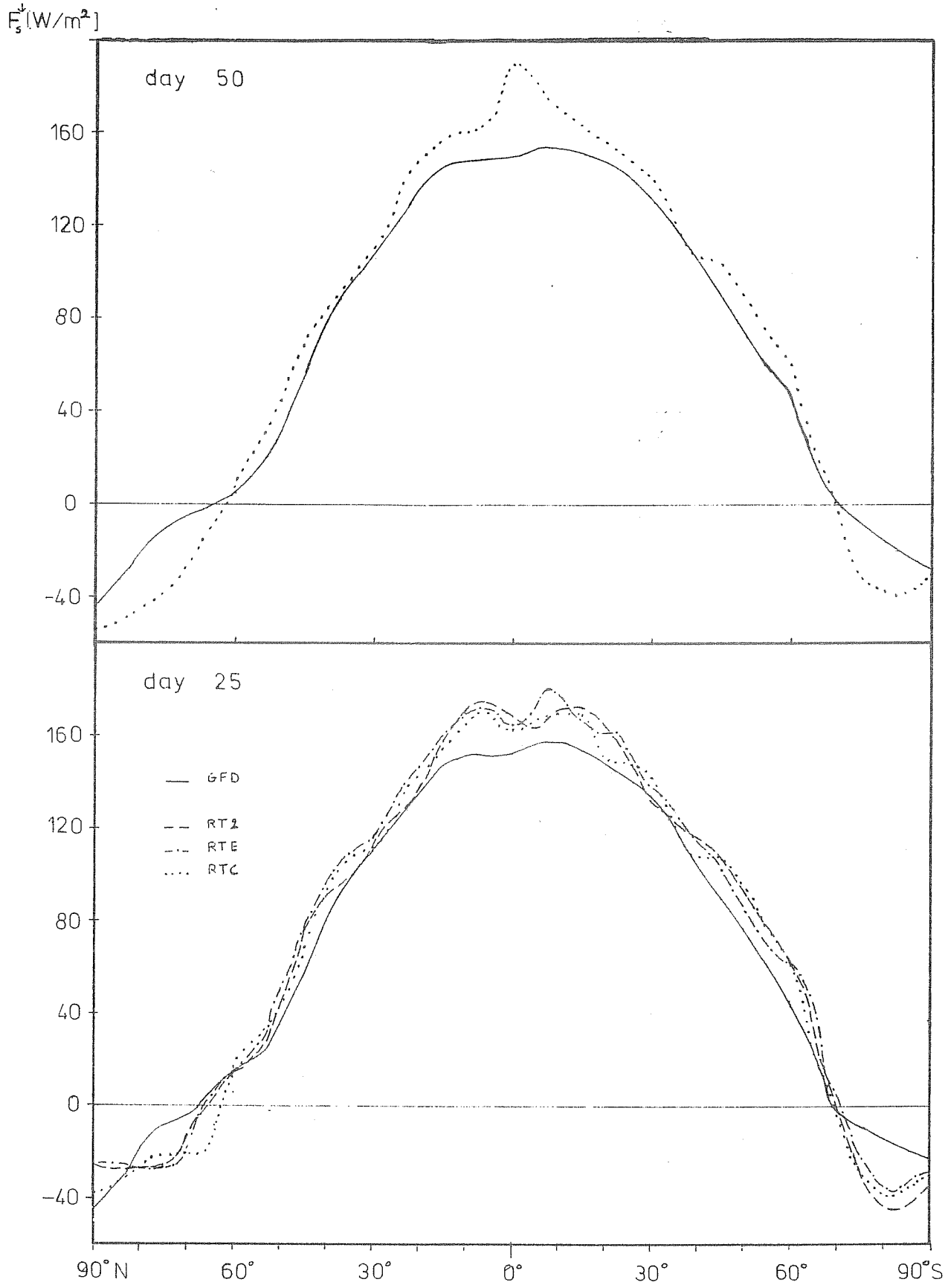
$F_s^{\downarrow}$[W/m²]
day 50
160
120
80
40
0
-40
day 25
GFD
RT2
RTE
RTC
90°N
60°
30°
0°
30°
60°
90°S

Figure 12

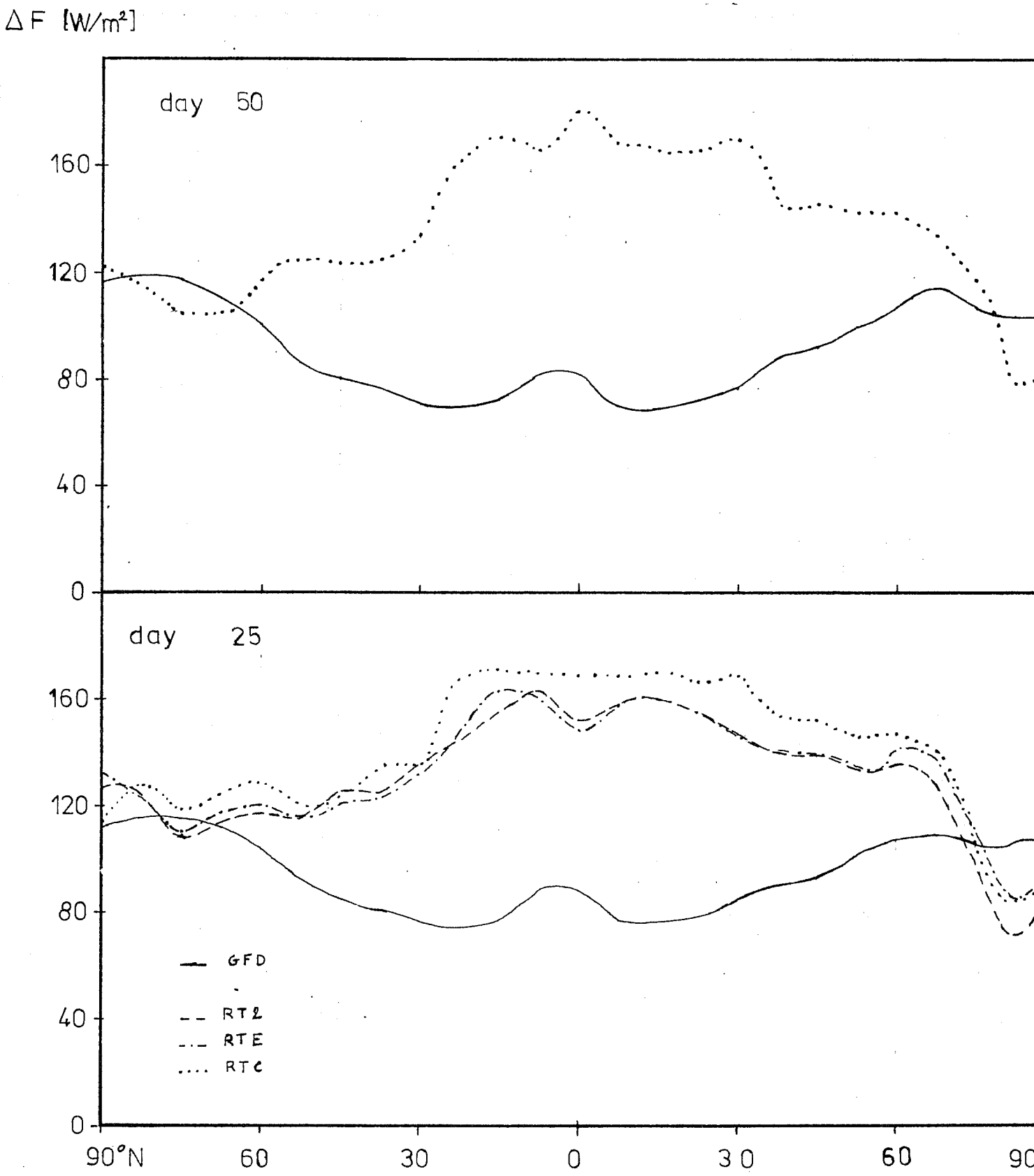
ΔF [W/m²]
day 50
160
120
80
40
0
day 25
160
120
80
40
0
GFD
RTL
RTE
RTC
90°N
60
30
0
30
60
90

Figure 13

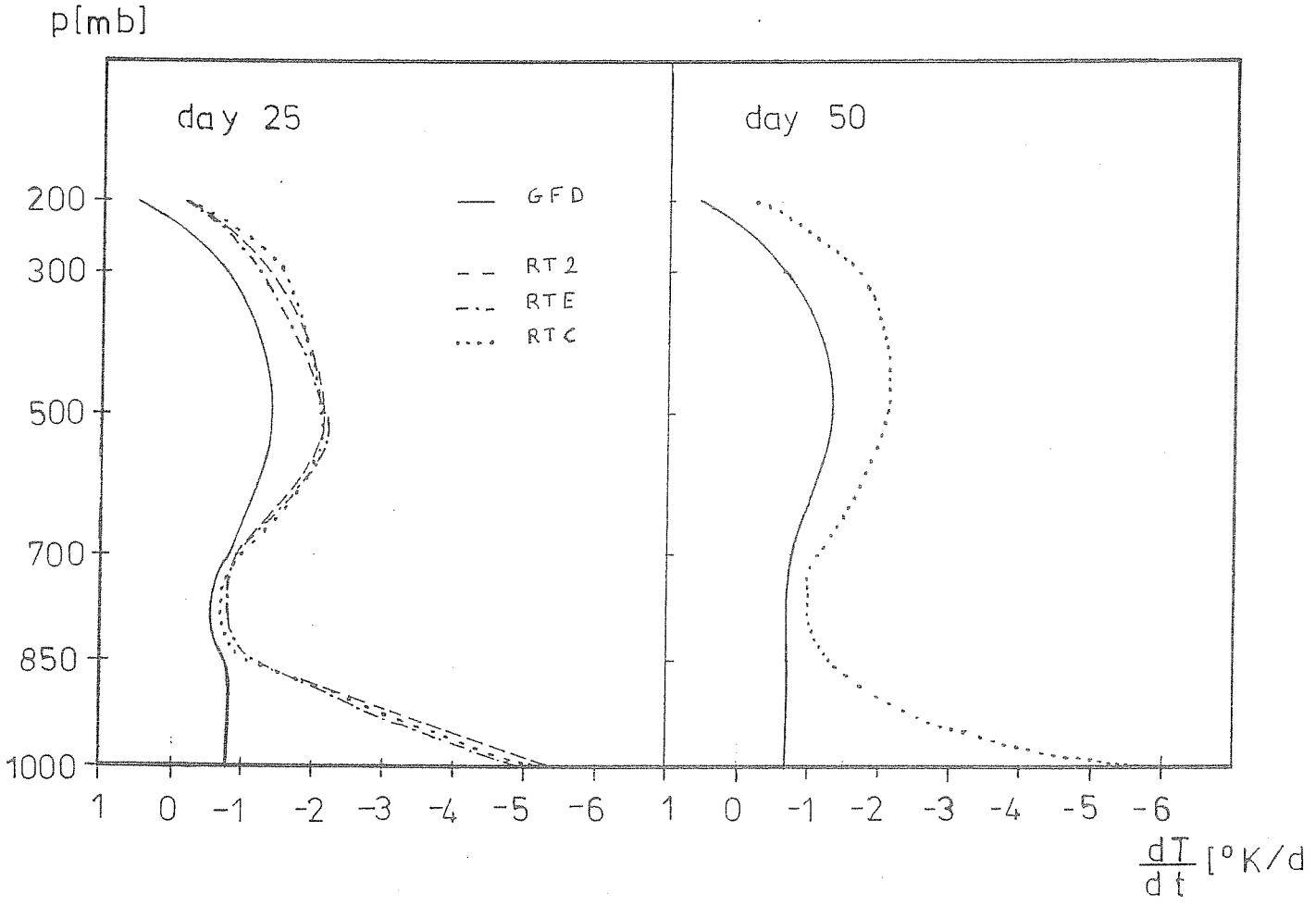
p[mb]
day 25
day 50
GFD
RT2
RTE
RTC
200
300
500
700
850
1000
1 0 -1 -2 -3 -4 -5 -6
1 0 -1 -2 -3 -4 -5 -6
dT/dt [°K/d]

Figure 14

REFERENCES:

Blondin, C.	1977	Analyse et adaptation d'un modèle de rayonnement en vue de son utilisation dans un modèle dynamique. Ecole Nationale de la Météorologie, Paris.
Brooks, D.L.	1950	A tabular method for the computation of temperature change of infrared radiation in the free atmosphere. J. Meteorol., 7, 313-321.
Elsasser, W.M.	1942	Heat Transfer by Infrared Radiation in the Atmosphere. Harvard Meteorological Studies, 6. Harvard University Press, Cambridge, Mass., 107pp.
Gamp, C. and Heinrich, M.	1976	Vergleich von gerechneten und gemessenen Divergenzprofilen des langwelligen Strahlungsflusses, Meteorol. Rundschau 29, 85-88.
Kano, M. and Miyauchi, M.	1977	On the comparison between the observed vertical profiles of longwave radiation fluxes and the computed ones in Japan. Papers on Meteorology and Geophysics, Vol.28/No.1, 1-8.
Katayama, A.	1974	A simplified scheme for computing radiative transfer in the troposphere. Technical Report No. 6, Dept. of Meteorology, UCLA.
London, J.	1952	The distribution of radiational temperature change in the northern hemisphere during March. J. Meteorol., 9, 145-151.
Louis, J.-F.	1977	Boundary Layer and Free Atmosphere. Proc., ECMWF Seminar.
Manabe, S. and Möller, F.	1961	On the radiative equilibrium and heat balance of the atmosphere. Mon. Weath. Rev., Vol.89, 503-532.

Manabe, S. and Strickler, R.F.	1964	Thermal equilibrium of the atmosphere with a convective adjustment. J. of Atmos. Sci., 21, 361-385.
McClatchey, R.A., Fenn, R.W., Selby, J.E., Volz, F.E. and Garing, J.S.	1972	Optical properties of the atmosphere. 3rd edition. AFCRL Environ. Res. Papers No. 411, 108pp.
McClatchey, R.A. Benedict, W.S., Clough, S.A., Burch, D.E., Calfee, R.F., Fox, K., Rothman, L.S. and Garing, J.S.	1973	AFCRL atmospheric absorption line parameters compilation. AFCRL Environ. Res. Papers No. 434, 78pp.
Paltridge, G.W. and Platt, C.M.R.	1976	Radiative Processes in Meteorology and Climatology. Elsevier Scientific Pub. Co.
Rodgers, C.D.	1977	Radiative Processes in the Atmosphere. Proc., ECMWF Seminar.
Rodgers, C.D. and Walshaw, C.D.	1966	The computation of infrared cooling rate in planetary atmospheres. Q.J.R. Meteorol. Soc., 92, 67-92.
Vigroux, E.	1953	Contribution à l'étude expérimentale de l'absorption de l'ozone. Annales de Phys. 8, p.709.
Walker, J.	1977	Technical Note/MetO20. Meteorological Office, Bracknell. (To be published).
Yamamoto, G.	1952	On a radiation chart. Sci. Rep. Tohoku Univ., Ser. 5,4: 9-23.
Yamamoto, G. and Onishi, G.	1953	A chart for the calculation of radiative temperature changes. Sci. Rep. Tohoku Univ., Ser. 5, Geophys., 4: 108.
Zdunkowski, W.G. Korb, G.J. and Nielsen, B.C.	1967	Prediction and maintenance of radiation fog. U.S. Army Electronics Command Report. Contr. DAAB 07-67-c-0049.